

MITOCHONDRIAL PROTEIN ACETYLATION AND LEFT VENTRICULAR FUNCTION IN
A MODEL OF HYPERTROPHIC CARDIOMYOPATHY AND HEART FAILURE

Amanda R. Stram

Submitted to the faculty of the University Graduate School
in partial fulfillment of the requirements
for the degree
Doctor of Philosophy
in the Department of Cellular and Integrative Physiology,
Indiana University

September 2017

Accepted by the Graduate Faculty of Indiana University, in partial fulfillment of the requirements for the degree of Doctor of Philosophy.

Doctoral Committee

R. Mark Payne, MD, Chair

Nickolay Brustovetsky, Ph.D.

B. Paul Herring, Ph.D.

May 23, 2017

Johnathan Tune, Ph.D.

© 2017

Amanda R. Stram

DEDICATION

To Brandon, Calvin and Anna.

ACKNOWLEDGEMENTS

Thank you, first and foremost, to Dr. R. Mark Payne for his unlimited support and mentorship over the years I have spent in his lab. He has been as generous with his academic guidance as with granting me autonomy to work and think independently. He is both an excellent scientist and clinician and it was a great honor to be a part of his team. I hope to be able to work with him on many more occasions in the future.

Second, I want to thank the members of my committee – Drs. Nickolay Brustovetsky, Paul Herring and Johnathan Tune - for their expertise, time, attention, and thoughtful contributions to my thesis as it evolved. I want to thank them especially for the detailed and enlightening scientific discussions that were so imperative for my transition from a clinician to a clinician-scientist.

Third, I want to thank the Department of Surgery, especially Dr. Gary Dunnington and Dr. Jennifer Choi, who were fully supportive of my time spent in academic pursuits in the lab, which kept me away from clinical duties and postponed my return to training. Their support has assured the first step toward my success as an active surgeon-scientist.

Fourth, I want to thank the Friedreich's Ataxia Research Alliance (FARA) community. It is the patients and families afflicted with FRDA, and their unwavering trust in scientific research for a cure, that keeps us motivated with the right perspective.

SOURCES OF FUNDING

This work was supported by an NIH/NHLBI NRSA fellowship grant #F31HL126489, grants from the Friedreich's Ataxia Research Alliance (FARA) and Muscular Dystrophy Association (MDA).

MITOCHONDRIAL PROTEIN ACETYLATION AND LEFT VENTRICULAR FUNCTION IN
A MODEL OF HYPERTROPHIC CARDIOMYOPATHY AND HEART FAILURE

Rationale: The childhood heart disease of Friedreich's Ataxia (FRDA) is characterized by hypertrophy and failure. It is caused by loss of frataxin (FXN), a mitochondrial protein involved in energy homeostasis. FRDA model hearts have increased mitochondrial protein acetylation and impaired sirtuin 3 (SIRT3) deacetylase activity. Protein acetylation is an important regulator of cardiac metabolism and SIRT3 is protective in heart disease. The underlying pathophysiology of heart failure in FRDA is unclear. I suspect that increased acetylation in FRDA heart mitochondria damages cardiac energy homeostasis by inhibiting activity of key enzymes involved in heart metabolism.

Objective: My project tested the hypothesis that altered acetylation of mitochondrial proteins contributes to the cardiomyopathy of FRDA.

Methods: Conditional mouse models of FRDA cardiomyopathy with ablation of FXN (FXN KO) or FXN and SIRT3 (FXN/SIRT3 DKO) in the heart were compared to healthy controls. Hearts were evaluated using echocardiography, cardiac catheterization, histology, protein acetylation and expression. FXN KO mice were treated with NAD⁺ replacement therapy with nicotinamide riboside (NR), and FXN/SIRT3 DKO mice were treated with FXN protein replacement therapy.

Results: Acetylation was temporally progressive and paralleled evolution of heart failure in the FXN KO model. High levels of acetylation were associated with cardiac fibrosis, mitochondrial damage, impaired fat metabolism, and diastolic and systolic dysfunction. Acetylation correlated

strongly with worse heart function, and loss of SIRT3 in the FXN KO mouse resulted in significant decrease in ejection fraction and fractional shortening. Treatment of the FXN/SIRT3 DKO with FXN protein therapy reduced acetylation but was not sufficient to fully rescue heart function. Increasing NAD⁺ with NR-treatment in the FXN KO lead to increased mitochondrial protein acetylation and did not improve cardiac outcome.

Conclusion: I found a strong negative correlation between heart function and mitochondrial protein acetylation. My findings also provide evidence that absence of SIRT3 expression in the FXN KO heart exacerbates features of heart failure, and that SIRT3 expression is necessary to rescue the FXN KO heart. These results suggest that SIRT3 inactivation and abnormal acetylation contribute to the pathophysiology of heart disease in FRDA.

R. Mark Payne, MD, Chair

TABLE OF CONTENTS

List of Tables	xii
List of Figures	xiii
List of Abbreviations	xiv
Chapter 1: Acetylation as a posttranslational modification of lysine residues on mitochondrial proteins and its implication in the heart disease of Friedreich’s Ataxia	1
Introduction	1
SIRT3 and lysine acetylation in mitochondria	2
Friedreich’s Ataxia hypertrophic cardiomyopathy and heart failure	5
Deregulation of Lysine Acetylation in Friedreich’s Ataxia Heart Failure	6
Conclusion	7
Chapter 2: Progressive Mitochondrial Protein Lysine Acetylation and Heart Failure in a Model of Friedreich’s Ataxia Cardiomyopathy	9
Introduction	9
Results	11
Cardiac hypertrophy and diastolic dysfunction are early and persistent findings in the FXN KO heart	11
FXN KO mice transition to dilated cardiomyopathy and heart failure	14
Acetylation is rapidly and temporally progressive and strongly correlates with a decline in heart function	16
Abnormal cardiac mitochondria ultrastructure is accompanied by mitochondrial respiratory inhibition	18
FXN KO hearts exhibit features of maladaptive ventricular remodeling	21
Loss of FXN in the heart leads to cardiac steatosis and cold	

intolerance	21
Discussion	25
Methods	27
Chapter 3: Loss of Sirtuin 3 Accelerates Heart Failure in a Murine Model of	
Friedreich’s Ataxia Mitochondrial Heart Disease	31
Introduction	31
Results	33
Subcellular location of protein acetylation	33
Acetylation in the FXN KO heart increases in the absence of SIRT3 expression	35
FXN KO and FXN/SIRT3 DKO hearts demonstrate abnormal cardiomyocyte mitochondria ultrastructure	37
Deletion of SIRT3 in the FXN KO heart increases cardiac fibrosis ...	37
Loss of SIRT3 increases protein acetylation and worsens heart failure in the FXN KO heart	38
Acetylated knockout hearts are hypertrophic with early diastolic dysfunction	39
FXN KO and FXN/SIRT3 DKO hearts have persistent diastolic dysfunction with a transition to dilated cardiomyopathy	40
Loss of SIRT3 in the FXN KO heart increases protein acetylation and worsens heart failure	41
Hypertrophic cardiomyopathy with conditional loss of SIRT3	41
Loss of SIRT3 in the FXN KO heart increases stress-related mortality and rate of heart failure-associated weight loss	48
NAD ⁺ replacement therapy with nicotinamide riboside increases mitochondrial protein acetylation and does not improve cardiac	

function in FXN KO mice	50
FXN protein replacement therapy	55
TAT-FXN protein replacement therapy in FXN/SIRT3 DKO mice is sufficient to decrease, but not normalize, mitochondrial protein acetylation	52
Discussion	54
Methods	57
Chapter 4: Conclusion	61
Appendices	
Appendix A	67
Appendix B	68
References	69
Curriculum vitae	

LIST OF TABLES

Table

2-1	Heart function as measured by left heart catheterization and echocardiography ...	13
3-1	Cardiac function measured by cardiac catheterization and echocardiography	43
3-2	Pairwise comparison of heart function between groups	44
3-3	Heart function of SIRT3 ^{fl/fl} and SIRT3 KO at 10 weeks	47

LIST OF FIGURES

Figure

1-1	Reversible Lysine Acetylation	3
2-1	FXN KO mice exhibit left ventricular hypertrophy and diastolic dysfunction and transition to dilated cardiomyopathy and heart failure	14
2-2	FXN KO mice exhibit diastolic dysfunction followed by dilated cardiomyopathy and heart failure	17
2-3	Figure 2-3. Acetylation is increased and progresses with age in FXN KO and correlates with worse heart function	19
2-4	Abnormal cardiac mitochondria ultrastructure is accompanied by respiratory inhibition in FXN KO hearts	20
2-5	FXN KO hearts exhibit features of maladaptive ventricular remodeling	23
2-6	Loss of FXN in the heart leads to cardiac steatosis and cold intolerance	24
3-1	Acetylation is increased in FXN/SIRT3 DKO hearts	34
3-2	Loss of SIRT3 increases cardiac fibrosis in the FXN KO heart	36
3-3	FXN KO and FXN/SIRT3 DKO heart function compared to controls	45
3-4	Loss of SIRT3 in FXN KO hearts exacerbates heart failure	46
3-5	Loss of SIRT3 in FXN KO hearts increases stress-related mortality and accelerates weight loss	49
3-6	Mitochondrial protein acetylation increases in response to NR treatment in FXN KO mice	51
3-7	No improvement in functional heart outcome in FXN KO mice after treatment with NR	52
3-8	FXN replacement in FXN/SIRT3 DKO mice reduces cardiac mitochondrial protein lysine acetylation	53

LIST OF ABBREVIATIONS

+dP/dt = left ventricle rate of contraction

-dP/dt = left ventricle rate of relaxation

AceCS2 = acetyl-CoA synthetase 2

BW = body weight

CI = electron transport chain complex I

CII = electron transport chain complex II

CIII = electron transport chain complex III

CV = electron transport chain complex V

CI = cardiac index

CO = cardiac output

E/A = mitral blood flow velocity ratio of *Early-to-Atrial* waves

EDP = end diastolic pressure

EDV = end diastolic volume

EF = ejection fraction

ESP = end systolic pressure

ESV = end systolic volume

ETC = electron transport chain

FS = fractional shortening

FRDA = Friedreich's Ataxia

FXN = frataxin

FXN^{f/f} = mouse line of healthy control littermates with floxed exon 4 of *Frda* gene

FXN KO = FXN MCK-Cre knockout mouse model

FXN/SIRT3 KO = FXN and SIRT3 MCK-Cre double knockout mouse model

GAPDH = glyceraldehyde 3-phosphate dehydrogenase

HMGCS2 = 3-hydroxy-3-methylglutaryl-CoA synthase 2

HR = heart rate

IDH2 = isocitrate dehydrogenase 2

IVRT = isovolumic relaxation time

LCAD = long-chain acyl-CoA dehydrogenase

LVIDd = left ventricular internal diameter in diastole

LVPWd = left ventricle posterior wall thickness in diastole

maxPwr = maximum power of left ventricle

MCAD = medium-chain acyl-CoA dehydrogenase

MHC = myosin heavy chain

Na = nicotinic acid

Nam = nicotinamide

NMN = nicotinamide mononucleotide

NR = nicotinamide riboside

OGG1 = 8-Oxoguanine glycosylase

PDH = pyruvate dehydrogenase

RCR = respiratory control ratio

RWT = relative wall thickness

SDHA = succinate dehydrogenase

SIRT3 = sirtuin 3

SIRT3^{fl/fl} = mouse line of healthy control littermates

SIRT3 KO = SIRT3 MCK-Cre knockout mouse model

SOD2 = superoxide dismutase 2

TAT = transactivator of transcription

TAT-FXN = FXN protein fused to TAT

Tau = left ventricle relaxation time constant

TCA = tricarboxylic acid cycle

VDAC = voltage-dependent anion channel

VLCAD = very-long-chain acyl-CoA dehydrogenase

CHAPTER 1

ACETYLATION AS A POSTTRANSLATIONAL MODIFICATION OF LYSINE RESIDUES ON MITOCHONDRIAL PROTEINS AND ITS IMPLICATION IN THE HEART DISEASE OF FRIEDREICH'S ATAXIA

Introduction

Heart failure carries a significant morbidity and mortality disease and cost burden in the United States (1). The underlying pathogenesis and molecular mechanism underlying heart failure is not well understood. Treatment modalities for heart failure consist of reducing symptoms and hospitalizations, yet it remains a progressive and frequently fatal disease (2). This highlights the importance of supporting scientific investigations that will illuminate the mechanisms responsible for heart failure.

Mounting evidence suggests that mitochondrial dysfunction is an important pathogenic mechanism for heart disease progression, such as that arising from hypertension, ischemia, and hypertrophic cardiomyopathy (3, 4). Mitochondrial protein acetylation is emerging as a critical post-transcriptional modification that acts to maintain normal mitochondrial function and heart metabolism (5). Sirtuin 3 (SIRT3) is a NAD⁺-dependent deacetylase that responds to intracellular metabolic cues and is activated in response to increased levels of NAD⁺. It is the only known protein responsible for mitochondrial deacetylation in the heart. Its targets include enzymes important to energy homeostasis, such as long chain acyl CoA (LCAD), pyruvate dehydrogenase (PDH), acetyl CoA synthetase 2 (AceCS2), and ATP synthase, among others (6).

Friedreich's Ataxia (FRDA) is a congenital mitochondrial disorder resulting in multisystem failure and early mortality in those afflicted (7, 8). The cardiac manifestation of FRDA results in hypertrophic cardiomyopathy progressing to heart failure. The heart disease of

FRDA appears to mimic the cellular, metabolic and physiologic adverse remodeling leading to heart failure that is common in other heart diseases. Specifically, left ventricle hypertrophy and a switch from oxidative metabolism to glycolysis are features of FRDA heart disease as well as prominent characteristics of evolving heart failure. FRDA heart failure is relentlessly progressive and there is no cure.

There is evidence that mitochondrial protein acetylation is deregulated in hearts of a murine model FRDA cardiomyopathy (9). This deregulation of acetylation arises from SIRT3 inhibition and results in hyperacetylation of protein lysine residues and mitochondrial dysfunction. Because SIRT3 is involved in key components of heart metabolism and mitochondrial integrity, it is likely that SIRT3 dysfunction and mitochondrial protein hyperacetylation play a key role in the cardiomyopathy of FRDA. Presented here is a summary of the emerging data on mitochondrial protein lysine acetylation and a discussion on the implication of abnormal acetylation in the childhood heart disease of FRDA.

SIRT3 and lysine acetylation in mitochondria

Sirtuins are a family of NAD^+ -dependent enzymes that regulate diverse biological functions. There are seven identified sirtuins, sirtuin 1-7, with three located in mitochondria, sirtuin 3-5. Sirtuin 3 (SIRT3) is a deacetylase that responds to cellular energy status and utilizes an “acetylation switch” to modify protein function (10-12). SIRT3 uses NAD^+ as a cofactor to catalyze the removal of acetyl groups from lysine side chains. Mitochondria appear to utilize lysine acetylation-deacetylation of proteins to respond quickly to metabolic cues and thus, acetylation represents an important post translational mechanism for maintaining normal mitochondrial function and metabolism (12).

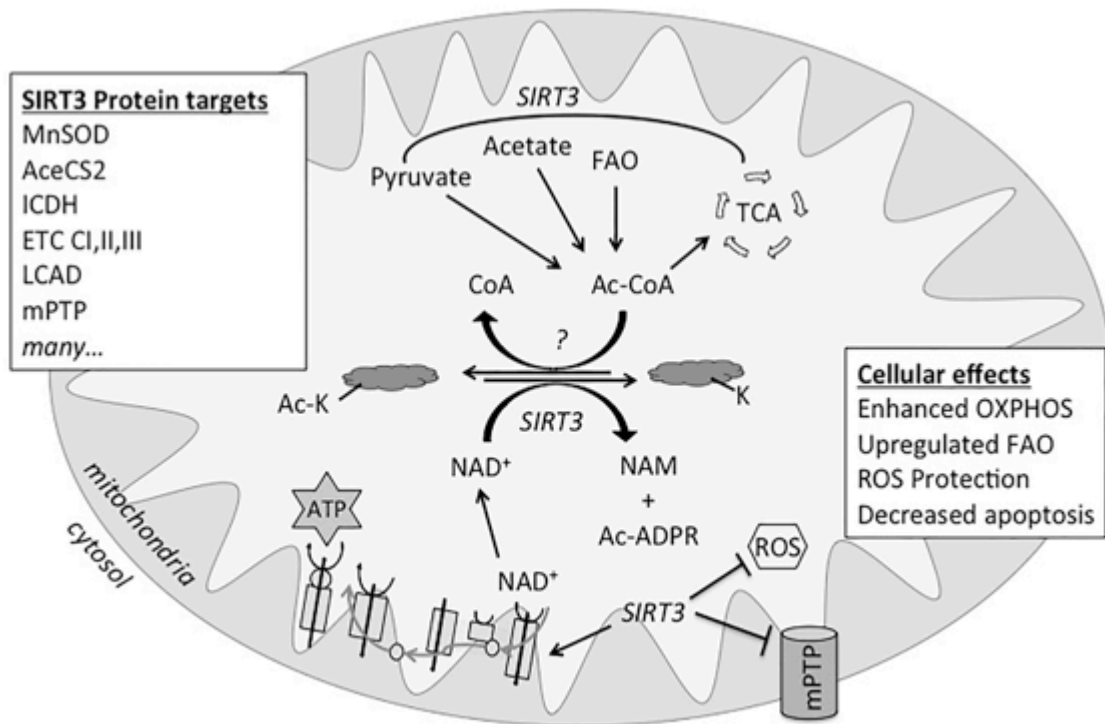


Figure 1-1. Reversible Lysine Acetylation. Mitochondrial protein lysine acetylation is regulated by the NAD^+ -dependent deacetylase, SIRT3. SIRT3 responds to mitochondrial energy and redox state to target proteins that, in turn, signal changes in cellular function. Ac-CoA = Acetyl-CoA; FAO = fatty acid oxidation; ? = no identified acetyltransferase enzyme; Ac-K = acetyl-lysine; K = lysine; NAM = nicotinamide; ADPR = ADP-Ribose; ROS = reactive oxygen species; mPTP = mitochondrial permeability transition pore.

While early reports suggested the presence of an acetyltransferase mechanism (13), definitive identification of such a counter enzyme has not been successful. Rather, acetylation appears to be non-enzymatic, and related to acetyl CoA availability and reactivity in the mitochondrial matrix (14, 15).

In general, SIRT3 protein targets are activated in response to removal of acetyl groups. Many SIRT3 targets are important to energy generation and utilization, such as long-chain acyl-CoA dehydrogenase (LCAD) (16, 17), pyruvate dehydrogenase (PDH) (18), acetyl-CoA synthetase 2 (AceCS2) (19), Isocitrate dehydrogenase 2 (IDH2) (20), and ETC complexes I-III and CV (ATP synthase)(21-24), among others important to core metabolic processes (6, 25-27) (Figure 1-1). SIRT3 deacetylation has been shown to increase the activity of energy-generating

enzymes in the electron transport chain. SIRT3 deacetylation activates CI-NDUFA9, CII-SDHA and ATP synthase (21, 22, 28, 29), thus SIRT3 acts directly to increase energy currency in the form of ATP and NAD⁺ in cells. Fatty acid metabolism, a major source of energy for the heart, is regulated by SIRT3 deacetylation of several enzymes including AceCS2, which stimulates conversion of acetate into acetyl CoA (19, 30), 3-hydroxy-3-methylglutaryl-CoA synthase 2 (HMGCS2) stimulating ketogenesis (31), and LCAD, stimulating fatty acid oxidation (17). Carbohydrate metabolism is regulated by deacetylation of cyclophilin D, releasing hexokinase 2 and causing a decrease in glycolysis (32), and PDH, which activates in response to deacetylation by SIRT3 (33).

SIRT3 also targets proteins that maintain physiologic redox balance and provide protection from oxidative damage. Deacetylation of superoxide dismutase 2 (SOD2) increases its activity as a free radical scavenger (34-36). IDH2 responds to deacetylation with increased metabolic activity in the TCA cycle, and is also associated with protection from oxidative stress-related cell death (20). Mitochondrial permeability transition pore-mediated apoptosis is also regulated by deacetylation, with deacetylation by SIRT3 inhibiting pore opening (25). Mitochondrial OGG1 (8-Oxoguanine glycosylase) stabilizes in response to deacetylation by SIRT3 under oxidative stress and protects from intrinsic apoptosis (37).

There is particular functional relevance of acetylation as a post-translational modification in cardiovascular disease. Given the heart's reliance on functional mitochondrial metabolism due to its constant demand for energy substrates, it is not surprising that SIRT3 is emerging as an important player in cardiovascular disease (38). For example, SIRT3 has been shown to protect against oxidative stress (39-41), attenuate fatty acid accumulation in the heart (42) and prevent development of stress-induced cardiac hypertrophy (43). Mice with ablation of SIRT3 have mitochondrial dysfunction resulting in myocardial energy loss, develop cardiac hypertrophy and fibrosis in response to mechanical stress (44), and are more susceptible to the detrimental effects of ischemia/reperfusion injury (45).

Friedreich's Ataxia hypertrophic cardiomyopathy and heart failure

The etiology of Friedreich's Ataxia (FRDA) arises from a homozygous GAA triplet expansion in the FXN gene (*Frda*) resulting in dysfunctional transcription and decreased expression of the FXN protein (46). Prevalence of FRDA is estimated at 1:29,000 -1:50,000, with a carrier frequency of 1:60-1:110 (8). FRDA manifests clinically as a multi-systemic disease with progressive neuronal degeneration, hypertrophic cardiomyopathy and endocrine disturbances, such as diabetes mellitus (46). Clinical symptom onset typically occurs in the second decade of life, with a mean age of death in the third or fourth decades (8, 47). Cardiac dysfunction is the most common overall cause of death and causes premature death in 60-80% of FRDA patients (48, 49). The detectable cardiac phenotype of FRDA results in abnormal electrocardiogram changes, arrhythmias, and left ventricular hypertrophy with severe interstitial fibrosis progressing to heart failure (50).

FXN is a highly conserved mitochondrial protein that functions in energy metabolism by acting as an iron binding protein in iron-sulfur enzyme biosynthesis, thus affecting multiple enzyme systems such as respiratory chain complexes I, II, and III, and aconitase of the TCA cycle (50-52). Diminished FXN expression results in mitochondrial dysfunction, impaired energy generation, decreased mitochondrial NAD^+/NADH ratios, and increased oxidative stress with a shift in the redox state (53). Under normal conditions, FXN expression is most robust in tissues enriched in mitochondria and with high metabolic demand, such as heart, liver, skeletal muscle, kidney and brown adipose tissue (46). In fact, FXN expression is highest in healthy heart tissue (54). FRDA patients have decreased myocardial levels of ATP, even in the absence of detectable contractile dysfunction, which underscores the importance of FXN in meeting energy needs. FXN-deficient cardiomyocytes show increased mitochondrial density, likely as a proliferative compensatory mechanism in response to inherent mitochondrial dysfunction (55).

The pathophysiology of FRDA cardiomyopathy remains under investigation, although it can be reasonably postulated that failing mitochondrial energetics contribute to clinical characteristics. There is no cure for FRDA and no methods are available to slow disease progression. Antioxidants and iron chelation have been investigated as therapeutic candidates, yet none have shown evidence of efficacy in clinical settings (56). Replacing FXN using viral gene therapy and targeted protein replacement show promise in animal studies. We are still far from understanding the exact function of FXN and the biochemical events leading to the pathophysiology of the cardiomyopathy of FRDA.

Deregulation of Mitochondrial Protein Lysine Acetylation in Friedreich's Ataxia Heart Failure

SIRT3 is inhibited in FXN-deficient heart mitochondria, causing global hyperacetylation of protein lysine residues as well as increased acetylation of specific targets of SIRT3, including LCAD and AceCS2 (9). Failure of SIRT3 to deacetylate important metabolic enzymes in response to existing energy needs will result in a paucity of metabolic substrates and, in turn, lead to mitochondrial metabolic dysfunction and presumably worsen the function of failing FXN-deficient mitochondria. The ratio of NAD^+/NADH is low in the FXN-deficient heart (9), likely because of dysfunctional mitochondrial oxidative metabolism that fails to oxidize NAD^+ from the available mitochondrial pool. Because SIRT3 deacetylase activity relies on the bioavailability of its required cosubstrate NAD^+ , the relative deficiency of NAD^+ is likely the key mechanism behind SIRT3 inhibition in FRDA hearts.

NAD^+ is a vital component of mitochondrial and cellular homeostasis, participating in oxidoreduction reactions for energy generation, as a cofactor for diverse enzymatic processes, and even acts as a signaling molecule. While the precise mechanisms that act to regulate NAD^+ in

the cell are still being explored, it is known that NAD⁺ can be regenerated via recycling of precursors of the vitamin B3 family, namely, nicotinic acid (Na), nicotinamide (Nam) and nicotinamide riboside (NR). In the mouse heart, the vast majority of NAD⁺ synthesized from precursors comes from Nam and NR, which are converted into nicotinamide mononucleotide (NMN) prior to entry into the mitochondria (57). Recent work in animal models has shown that exogenous treatment with either NR or NMN can boost NAD⁺ levels in mitochondria and activate sirtuins (58-61). NAD⁺ replacement therapy has garnered special attention in recent years as an attractive therapeutic potential for pharmacological modulation of protein lysine acetylation to improve cardiac metabolism and physiologic function. In the FXN-deficient heart, recovering diminished NAD⁺ levels could alleviate inhibition of SIRT3 to reinstate its diverse protective effects on the heart. In fact, reversal of hyperacetylation in FXN-deficient cells can be achieved by replacing NAD⁺ together with SIRT3 *in vitro* (9). It remains to be shown whether such supplementation is similarly efficacious in such cells *in vivo*, and would be of great interest to pursue.

Conclusion

The rapid and recent increase in knowledge of protein acetylation as a post-translational processing mechanism with metabolically-enriched mitochondrial targets has lead to a tremendous amount of new information on the mitochondrial orchestration of cellular energy and metabolism. The functional significance of many of these post-translational modifications in the mitochondria, in regard to their impact in the pathophysiology of disease, has not been fully explored and needs to be delineated further. However, it is evident that protein signaling via reversible protein modifications is widely and extensively used in mitochondria as a mechanism to respond to shifts in nutrient and redox status. Given the fundamental role of mitochondria in

providing energy and regulating metabolic homeostasis of the cell, and especially in the heart, and the close link between mitochondrial dysfunction and disease, ongoing investigations will likely continue to yield clues to functional significance. Mitochondrial protein modifications show promise for use as modifiable mitochondrial targets for therapies aimed to regulate cardiac metabolism in an attempt to alleviate the burden of heart disease.

CHAPTER 2

PROGRESSIVE MITOCHONDRIAL PROTEIN LYSINE ACETYLATION AND HEART FAILURE IN A MODEL OF FRIEDREICH'S ATAXIA CARDIOMYOPATHY (62)

Introduction

Heart disease and heart failure exert a significant morbidity and mortality burden worldwide. Abnormal metabolism and metabolic remodeling are common pathologic features in heart disease, such as in obesity and diabetes-related cardiomyopathy (63, 64), ischemia (65), and heart failure (4, 66). Mitochondrial dysfunction and heart disease are closely linked (67), and because mitochondria are central to regulating cellular energy and fulfilling the high demands of cardiac metabolism, it is expected that mitochondrial dysfunction plays a key pathologic role in abnormal cardiac metabolism (68).

Mitochondrial protein acetylation is an important post-translational regulatory mechanism of heart metabolism that has emerged in recent years. Acetylation in mitochondria is controlled by the NAD⁺-dependent deacetylase, sirtuin 3 (SIRT3). SIRT3 responds to cellular energy status and utilizes an “acetylation switch” to modify protein function (11) in order to respond quickly to metabolic cues and thus, operates a chief mechanism for maintaining normal mitochondrial function and metabolism (12). SIRT3 targets enzymes that are typically activated in response to removal of acetyl groups, and which are important to energy generation and utilization, such as very-long-chain, long-chain, and medium-chain acyl-CoA dehydrogenases (VLCAD, LCAD and MCAD) (16, 69), pyruvate dehydrogenase (PDH) (18), acetyl CoA synthetase 2 (AceCS2) (19), and electron transport chain (ETC) complexes I-III (22, 24, 70). Additionally, SIRT3 appears to deacetylate other important proteins, such as those that provide protection from oxidative damage, e.g., superoxide dismutase 2 (SOD2) (34). It is worth noting

here that enzyme response to acetylation state is an area of continuing investigation. For instance, others have reported an increase in activity in LCAD in response to acetylation, specifically in obesity-related heart disease (71).

Beneficial effects of SIRT3 activity in the heart are well documented. For example, SIRT3 has been shown to protect against oxidative stress, attenuate fatty acid accumulation in the heart (42), and prevent development of stress-induced cardiac hypertrophy (72). Mice lacking SIRT3 have mitochondrial dysfunction eventually resulting in myocardial energy loss, develop hypertrophy and fibrosis in response to mechanical stress (44), and are more susceptible to the detrimental effects of ischemia/reperfusion injury (45).

Acetylation is most exciting in the context of heart disease in that it has potential as a therapeutically modifiable target. For example, recent work has shown that exogenous treatment with NAD⁺ precursors can increase NAD⁺ levels in mitochondria, activate sirtuins to reduce protein acetylation, and improve cardiac outcome (58, 59).

The heart disease of Friedreich's Ataxia (FRDA) results from inherited deficiency of frataxin (FXN), a mitochondrial protein important in energy homeostasis. FXN is a highly conserved mitochondrial matrix protein that functions in iron-sulfur cluster assembly, which is integral to mitochondrial metabolic machinery (73). Reduced expression of FXN in FRDA results in impaired energy generation, a decreased NAD⁺/NADH ratio, and increased oxidative stress (74-76). In addition to ataxia, patients often develop hypertrophic cardiomyopathy and heart failure. The vast majority of patients who go on to develop cardiomyopathy are asymptomatic until late stages of disease. The most frequent cause of mortality in FRDA arises from cardiac etiology, most commonly due to congestive heart failure (48). There is no known cure.

Mice with conditional loss of FXN in the heart develop cardiac hypertrophy as early as 5 weeks of age, followed by transition to dilated cardiomyopathy and heart failure by approximately 8 weeks of age (77). Certain biochemical and structural changes occur in the FRDA mouse model heart as early as 4 weeks of age, including reduced activity of important

metabolic enzymes (such as those of the ETC complexes and aconitase) and mitochondrial ultrastructure abnormalities (77). The importance of these findings is that underlying changes in the FRDA heart originate prior to overt abnormalities in cardiac function and thus, may present a window of opportunity for intervention before irreversible changes occur.

We previously reported that mitochondrial proteins in FRDA mouse model hearts have increased acetylation and decreased SIRT3 activity, resulting in increased acetylation of several important metabolic enzymes, including LCAD, MCAD, AceCS2, and the ETC (76, 78). The reduction in SIRT3 activity is likely due to insufficient NAD⁺ bioavailability as a result of dysfunctional energy metabolism, and possibly by direct oxidative modification of the native protein. The impact of abnormal acetylation in the FRDA heart has not been investigated. Because of the important role that acetylation plays in cardiac function, we believe that loss of SIRT3 and resultant mitochondrial protein hyper-acetylation contributes to the heart disease of FRDA.

The purpose of the present study was to document the changes in physiology and function that evolve over time in a model of FRDA heart failure using both non-invasive (ECHO) and invasive left heart catheterization, and match the trajectory of cardiac pathophysiology to the protein acetylation profile along the course of disease in order to determine the link between acetylation of mitochondrial proteins and FRDA heart disease.

Results

Cardiac hypertrophy and diastolic dysfunction are early and persistent findings in FXN KO hearts

We used an established conditional mouse model of FRDA heart failure with absence of FXN in the heart (FXN MCK-Cre KO, referred to here as “FXN KO”) compared to healthy

littermates (FXN^{fl/fl}) (79). We examined cardiac function in detail, using ECHO and invasive left heart catheterization at postnatal age day 30 ±5, 45 ±4 and 65 ±5. These groups represented pre-, mid- and late heart disease according to previous reports (77). There were no functional or anatomic differences between hearts of FXN KO and control mice at day 30 (Table 2-1).

Cardiac hypertrophy is manifest by day 45 in FXN KO animals (Table 2-1, Figure 2-1). Compared to controls, day 45 FXN KO mice have thickened left ventricular (LV) posterior walls in diastole (LVPWd) (FXN KO = 0.82 ±0.12 mm vs. FXN^{fl/fl} = 0.64 ±0.08 mm; $p < 0.001$), increased relative wall thickness (RWT) (FXN KO = 0.42 ±0.07 vs. FXN^{fl/fl} = 0.33 ±0.05; $p = 0.002$). FXN KO at day 45 also show findings consistent with both cardiomegaly and hypertrophy with increased ECHO-derived LV:body (FXN KO = 5.1 ±0.9 vs. FXN^{fl/fl} = 3.9 ±0.7; $p = 0.004$) and gross heart (mg):body weight (g) ratios (FXN KO: 5.90 ±1.70 vs. FXN^{fl/fl}: 4.41 ±0.42; $p = 0.021$).

Diastolic dysfunction occurs early, is concomitant with presentation of LV hypertrophy, and is persistent in FXN KO hearts. FXN KO mice demonstrate multiple relaxation abnormalities at day 45 (Table 2-1, Figure 2-1 & 2-2). Mitral blood flow velocity ratio of *Early-to-Atrial* waves (E/A) on Doppler imaging is increased at day 45 (FXN KO = 2.4 ±0.8 vs. FXN^{fl/fl} = 1.5 ±0.2; $p = 0.003$) and 65 (FXN KO = 3.7 ±1.4 vs. FXN^{fl/fl} = 1.4 ±0.2; $p < 0.001$), as well as isovolumic relaxation time (IVRT) at day 45 (FXN KO = 26.8 ±1.2 ms vs. FXN^{fl/fl} = 23.9 ±2.3 ms; $p = 0.008$) and day 65 (FXN KO = 33.6 ±4.2 ms vs. FXN^{fl/fl} = 21.9 ±2.5 ms; $p < 0.001$). Left ventricle relaxation rate (-dP/dt) is decreased in FXN KO compared to controls at days 45 (FXN KO = -6,087 ±1,378 mmHg/sec vs. FXN^{fl/fl} = -9,704 ±799 mmHg/sec; $p < 0.001$) and 65 (-4,099 ±1,104 mmHg/sec vs. FXN^{fl/fl} = -9,228 ±891 mmHg/sec; $p < 0.001$). Finally, Tau, the LV relaxation time constant, is increased in FXN KO compared to controls at both day 45 (Tau Weiss: FXN KO = 7.81 ±1.22 vs. FXN^{fl/fl} = 4.53 ±0.57 ms, $p < 0.001$) and 65 (Tau Weiss: FXN KO = 7.81 ±0.95 vs. FXN^{fl/fl} = 4.99 ±0.50 ms, $p < 0.001$), demonstrating prolonged relaxation phase in diastole.

Heart function as measured by left heart catheterization and echocardiography						
	30		45		65	
	<u>FXN^{fl/fl}</u> n = 7	<u>FXN KO</u> n = 9	<u>FXN^{fl/fl}</u> n=7	<u>FXN KO</u> n=6	<u>FXN^{fl/fl}</u> n=7	<u>FXN KO</u> n=7
<i>CATH</i>						
Age (day)	30.7 ±1.8	31.9 ±2.9	46.9 ±0.9	44.8 ±0.4**	63.6 ±3.8	64.6 ±3.4
HR (bpm)	605.3 ±85.3	577.1 ±44.6	671.4 ±95.2	580.9 ±81.4	595 ±77.1	643.3 ±105.2
EF (%)	56.0 ±9.8	49.7 ±7.4	40.9 ±11.8	48.8 ±6.7	50.2 ±6.1	25.2 ±9.5***
+dP/dt (mmHg/s)	1015 ±1848	8760 ±962	11882 ±1928	6875 ±1156***	10809 ±1591	5165 ±1101***
-dP/dt (mmHg/s)	-8114 ±1067	-7802 ±817	-9704 ±799	-6087 ±1378***	-9228 ±891	-4099 ±1104***
MaxPwr	107.5 ±31.2	84.7 ±14.5	143.3 ±32.1	67.5 ±20.7***	121.2 ±31.5	37.3 ±14.1***
Tau (Weiss) (ms)	5.3 ±1.0	5.6 ±0.5	4.5 ±0.6	7.8 ±1.2***	5.0 ±0.5	7.8 ±1.0***
Tau (Mirsky) (ms)	8.7 ±1.5	8.4 ±1.0	8.4 ±0.9	11.0 ± 1.3**	8.6 ± 1.0	10.9 ± 1.5**
ESP (mmHg)	88.6 ±10.2	87.4 ±9.7	103.2 ±5.4	87.7 ±11.9*	99.5 ±7.3	65.2 ±11.0***
EDP (mmHg)	11.7 ±4.5	11.0 ±3.3	10.9 ±3.8	13.0 ±5.7	8.8 ±3.0	10.0 ±5.3
ESV (μl)	22.9 ±7.9	23.1 ±5.1	26.6 ±10.7	24.8 ±5.9	26.8 ±6.9	74.7 ±15.7***
EDV (μl)	50.9 ±6.6	45.7 ±7.3	43.6 ±12.2	48.2 ±9.0	53.4 ±7.8	99.6 ±15.2***
	<u>FXN^{fl/fl}</u> n=10	<u>FXN KO</u> n=10	<u>FXN^{fl/fl}</u> n=11	<u>FXN KO</u> n=10	<u>FXN^{fl/fl}</u> n=9	<u>FXN KO</u> n=9
<i>ECHO</i>						
BW (g)	15.6 ±3.0	13.5 ±3.7	20.4 ±2.0	21.3 ±1.7	23.7 ±2.4	22.4 ±1.2
EF (%)	55.0 ±10.1	54.2 ±7.3	49.9 ±13.7	45.9 ±8.0	47.7 ±8.2	23.9 ±12.5***
FS (%)	28.2 ±6.4	27.6 ±5.0	25.6 ±9.2	22.7 ±4.6	23.7 ±4.9	11.1 ±6.0***
CO (ml/min)	19.7 ±7.2	18.9 ±8.1	17.4 ±5.1	16.8 ±4.6	21.4 ±4.9	13.2 ±5.1*
CI (ml/min/g)	1.2 ±0.3	1.4 ±0.4	0.87 ±0.27	0.80 ±0.24	0.89 ±0.16	0.58 ±0.23*
LVIDd (mm)	3.6 ±0.3	3.6 ±0.4	3.9 ±0.3	3.9 ±0.4	3.91 ±0.14	4.49 ±0.56**
LVPWd (mm)	0.61 ±0.12	0.58 ±0.14	0.64 ±0.08	0.82 ±0.12***	0.62 ±0.13	0.85 ±0.22*
RWT	0.35 ±0.10	0.32 ±0.10	0.33 ±0.05	0.42 ±0.07**	0.32 ±0.07	0.39 ±0.13
LV:body	4.1 ±1.4	4.5 ±1.6	3.9 ±0.7	5.1 ±0.9**	3.47 ±0.70	5.71 ±1.19***
E/A	1.6 ±0.2	1.7 ±0.2	1.5 ±0.2	2.4 ±0.8**	1.4 ±0.2	3.7 ±1.4***
IVRT (ms)	25.1 ±3.0	23.6 ±3.4	23.9 ±2.3	26.8 ±1.2**	21.9 ±2.5	33.6 ±4.2***

Table 2-1: Heart function as measured by ECHO and invasive left heart catheterization for FXN KO and controls at ages 30, 45 and 65 days. *= $p < 0.05$, **= $p < 0.01$, ***= $p < 0.001$. HR = heart rate; EF = ejection fraction; +dP/dt = rate of contraction; -dP/dt = rate of relaxation; maxPwr = maximum power left ventricle; Tau (Weiss) = regression of log(pressure); Tau (Mirsky) = time required for LV pressure to fall to one-half of its value at end systolic pressure; ESP = end systolic pressure; EDP = end diastolic pressure; ESV = end systolic volume ; EDV = end diastolic volume; BW = body weight; FS = fractional shortening; CO = cardiac output; CI = cardiac index; LVIDd = LV internal diameter in diastole; LVPWd = LV posterior wall thickness in diastole; RWT = relative wall thickness; E/A = mitral blood flow velocity ratio of Early-to-Atrial waves; IVRT = isovolumic relaxation time.

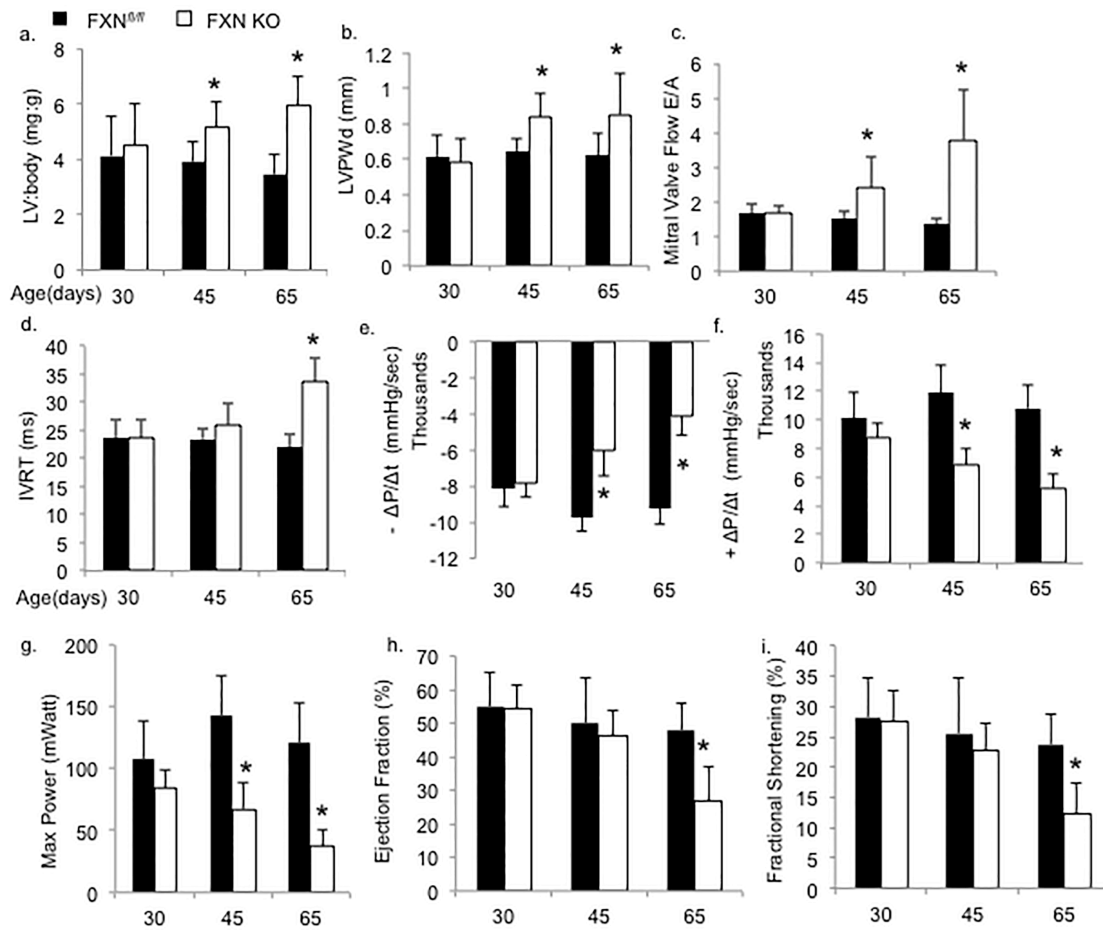


Figure 2-1. FXN KO mice exhibit left ventricular hypertrophy and diastolic dysfunction and transition to dilated cardiomyopathy and heart failure. FXN KO mice demonstrate cardiac hypertrophy at ages 45 and 65 days on (a) ECHO-derived left ventricle:body mass ratio (LV:body) and (b) left ventricular posterior wall thickness in diastole (LVPWd). Diastolic indices in the FXN KO mice are abnormal; with increases in (c) mitral valve Doppler flow ratio (E/A) and (d) isovolumic relaxation time (IVRT), and (e) decreased rate of left ventricle relaxation (-dP/dt). (f) FXN KO (days 45 and 65) had significantly slower rates of contraction (+dP/dt) and (g) maximum left ventricular power (maxPower) compared to FXN^{fl/fl} controls. (h) FXN KO mice demonstrate significantly depressed global contractility function compared to controls for ejection fraction (EF, %) and (i) fractional shortening (FS, %). E/A = ratio of the early (E) to late (A) ventricular filling velocity; -dP/dt = -Δintra-ventricular pressure/Δtime; +dP/dt = +Δintra-ventricular pressure/Δtime. *=*p*<0.05

FXN KO mice transition to dilated cardiomyopathy and heart failure

Contractility abnormalities occur in FXN KO mice as early as postnatal day 45 on invasive measurements, with progressive decline in systolic indices on day 65 measurements

(Table 2-1, Figure 2-1 & 2-2). At day 45, FXN KO mice have a significant decrease in maximum ventricular power (maxPower) compared to controls (FXN KO = 67.5 ± 20.7 mWatt vs. FXN^{fl/fl} = 143.3 ± 32.1 mWatt; $p < 0.001$) as well as rate of contraction (+dP/dt) (FXN KO = $6,875 \pm 1,155$ mmHg/sec vs. FXN^{fl/fl} = $11,882 \pm 1,928$ mmHg/sec; $p < 0.001$). Again, at day 65, FXN KO mice demonstrate significantly depressed contractility (+dP/dt) ($5,165 \pm 1,100$ mmHg/sec) compared to control mice ($10,809 \pm 1,591$ mmHg/sec) ($p < 0.001$) in addition to decreased maxPower (FXN KO = 37.3 ± 14.1 mWatt vs. FXN^{fl/fl} = 121.2 ± 31.5 mWatt; $p < 0.001$).

FXN KO mice progress to overt systolic heart failure on ECHO by postnatal day 65. Compared to controls, FXN KO animals have significantly reduced EF (FXN KO = $23.9 \pm 12.5\%$ vs. FXN^{fl/fl} = $47.7 \pm 8.2\%$, $p < 0.001$) and fractional shortening (FS) (FXN KO = $11.1 \pm 6.0\%$ vs. FXN^{fl/fl} = $23.7 \pm 4.91\%$, $p < 0.001$). FXN KO mice at day 65 also demonstrate reductions in both cardiac output (CO) (FXN KO = 13.2 ± 5.1 ml/min vs. FXN^{fl/fl} = 21.4 ± 4.9 ml/min, $p = 0.010$) and cardiac index (CI) (FXN KO = 0.58 ± 0.23 ml/min/g vs. FXN^{fl/fl} = 0.89 ± 0.16 ml/min/g, $p = 0.014$) compared to controls.

Consistent with previous reports (77, 79), dilated cardiomyopathy is present in the FXN KO at day 65. There is a significant increase in LV internal diameter in diastole (LVIDd), in FXN KO (4.49 ± 0.56 mm) compared to FXN^{fl/fl} (3.91 ± 0.14 mm) ($p = 0.006$), providing evidence of a dilated LV. Further, the end-cycle blood volumes of the chamber in diastole are markedly increased in FXN KO at 65 days. Left ventricle end-diastolic volume (EDV) data collected with catheter-based direct volume measurements show that day 65 FXN KO mice have an increased EDV that is almost twice that of FXN^{fl/fl} (99.7 ± 15.2 μ l vs. 52.7 ± 8.29 μ l, respectively; $p < 0.001$), causing a dramatic rightward-shift in their pressure-volume curves (Table 2-1, Figure 2-2).

FXN KO mice at 65 days of age maintain earlier findings of cardiomegaly on ECHO-derived LV:body weight ratios (5.71 ± 1.19) compared to FXN^{fl/fl} mice (3.47 ± 0.70) ($p < 0.001$). FXN KO mice at day 65 also demonstrated close to a 50% increase in gross heart:body weight

ratio (8.81 ± 1.5) than that measured at day 45 (5.90 ± 1.7), and significantly higher than age-matched controls (4.70 ± 0.26) ($p < 0.001$) (Table 2-1, Figure 2-1).

Acetylation is rapidly and temporally progressive and strongly correlates with a decline in heart function

We previously demonstrated that acetylation in the conditional FXN KO heart is dramatically increased in late stages of heart disease and that the majority of protein acetylation was localized to mitochondria (76). Here, we examined the level of lysine acetylation in heart tissue at each time point in which we measured cardiac function in order to determine the level of cardiac protein lysine acetylation relative to the evolution of cardiac dysfunction from pre-disease to overt heart failure.

We show that acetylation is modestly increased prior to onset of detectable cardiac dysfunction in the FXN KO heart at day 30. This is followed by a dramatically rapid and progressive increase in protein acetylation compared to controls (2-3a). We measured the expression levels of several essential mitochondrial electron transport proteins, and as expected, based on the established role of FXN in Fe-S cluster enzyme assembly (73, 80) and prior studies (76), the expression of ETC complex subunits CI-NDUFA9, CII-SDBH and CIII-Rieske is reduced in FXN KO and decreases consistently over this time course (Figure 2-3).

Surprisingly, when the level of acetylation was correlated with measured cardiac function, there was a strong inverse correlation between amount of acetylation, as measured by relative density on western blot imaging, and EF ($r = -0.923$) and FS ($r = -0.927$) (Figure 2-3). To demonstrate that mitochondrial deacetylase activity is decreased or absent in the FXN KO hearts, we probed for acetylation of known SIRT3 mitochondrial protein targets, SOD2 and LCAD.

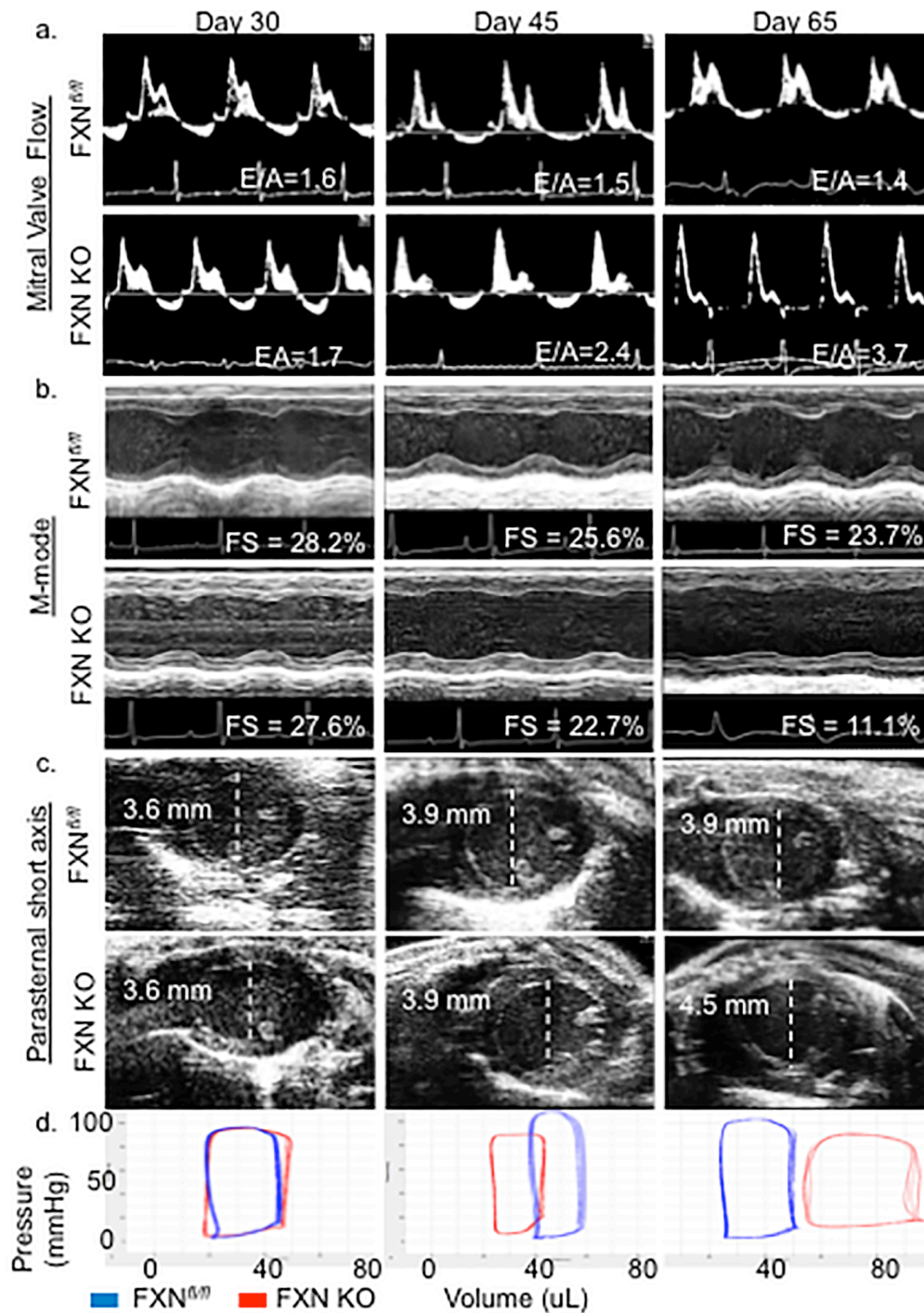


Figure 2-2. FXN KO mice exhibit diastolic dysfunction followed by dilated cardiomyopathy and heart failure. (a) Representative mitral valve Doppler flow patterns (ratio of the early (E) to late (A) ventricular filling velocity, E/A) demonstrate restrictive cardiomyopathy in FXN KO at days of age 45 and 65. (b) Echocardiographic parasternal short axis M-mode images demonstrate progressive impairment in left ventricle wall movement with decreased fractional shortening (FS) in FXN KO. (c) Parasternal axial images illustrate dilated cardiomyopathy with increased left ventricular internal diameter in diastole (LVIDd) in FXN KO at day 65. (d) FXN KO pressure volume loops represent increased end-diastolic volume (EDV) at day 65 compared to controls ($p < 0.001$) with notable rightward shift of pressure-volume curves. Values indicated in (a), (b) and (c) are averages per group.

SOD2 acts to destroy superoxide radicals and is inhibited when acetylated at lysine 68. SIRT3 reverses acetylation (34, 81). LCAD is a key enzyme in fatty acid oxidation and reports have demonstrated increased activity in response to deacetylation by SIRT3 (39, 82). As expected, we detected increased acetylation of both SOD2 and LCAD in the FXN KO compared to controls (Figure 2-3), confirming decreased activity of SIRT3 deacetylase. These results are consistent with prior studies in our lab that demonstrated hyper-acetylation of SIRT3 targets in cardiac-specific FXN KO hearts, including AceCS2, LCAD, and MCAD (78).

Abnormal cardiac mitochondria ultrastructure is accompanied by mitochondrial respiratory inhibition

Consistent with previous reports (55, 77), we found that pathologic changes in mitochondria become evident on electron microscopy (EM) as early as postnatal day 30 in ventricular tissue of FXN KO, and increase in prevalence over time (Figure 2-4). Mitochondrial ultrastructure changes in FXN KO hearts include loss and collapse of cristae, disordered mitochondria-to-sarcomere arrangement, and extensive accumulation and stacking of mitochondria, in addition to widespread electron-dense inclusions at day 65.

We quantified these observed morphological changes by measuring the ratio of myofibril-to-mitochondria area from micrographs, and determined the percentage of abnormal mitochondria in each strain (83). At day 65, the myofibril-to-mitochondria ratio was significantly decreased in FXN KO (0.90 ± 0.46) compared to controls (1.89 ± 0.47) ($p=0.011$), and the average percentage of mitochondrial area containing abnormal mitochondria in FXN KO

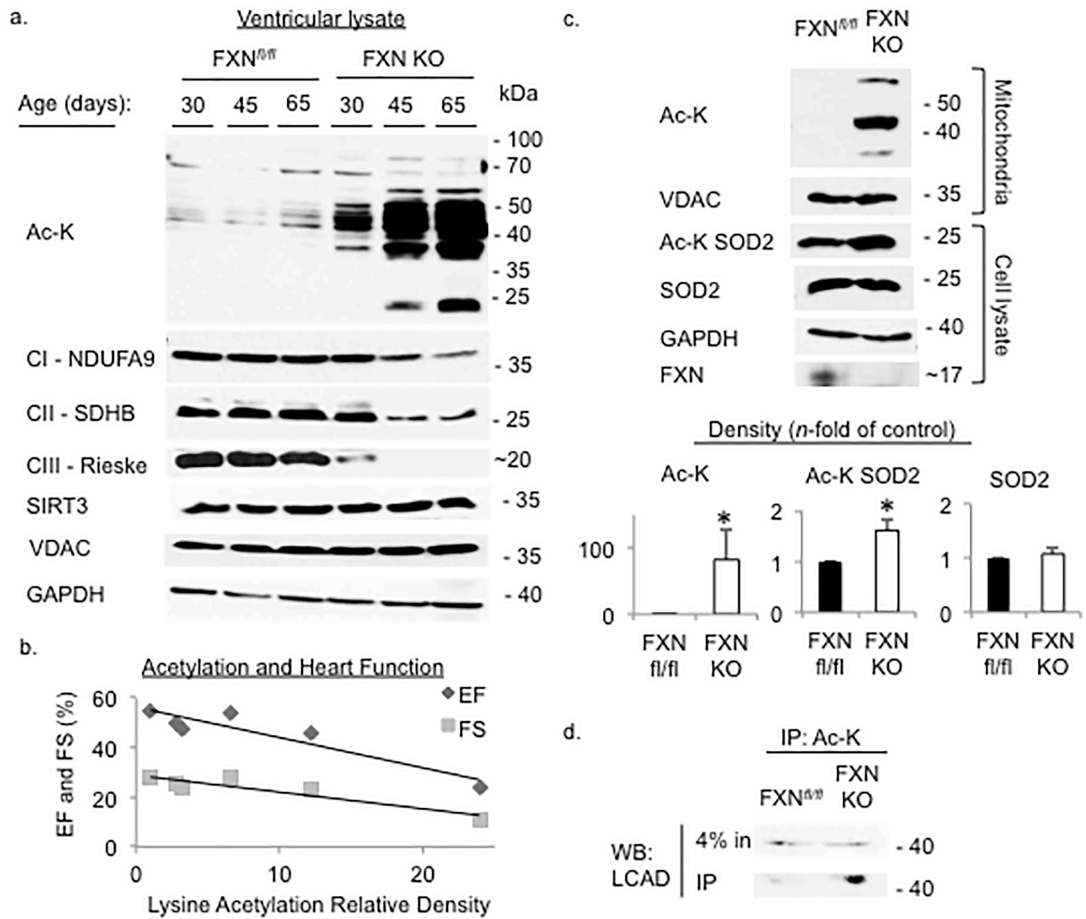


Figure 2-3. Acetylation is increased and progresses with age in FXN KO, and correlates with worse heart function. Whole cell preparations or mitochondrial isolates from ventricular tissue were probed for proteins of interest as indicated. (a) Acetylation of lysine residues is increased early and progresses with age, and expression of electron transport chain complex subunits decreases in FXN KO hearts. (b) Plot of correlation between acetylation and systolic indices of heart function shows negative correlation between level of acetylation and ventricular function. (c) FXN hearts at day 65 had significantly increased total mitochondrial protein lysine acetylation ($p=0.0339$), increased acetylation of SOD2 at Lys-68 (AcK-SOD2) ($p=0.0016$) and (d) increased acetylation of LCAD compared to controls ($p=0.0291$). EF = ejection fraction, FS = fractional shortening.

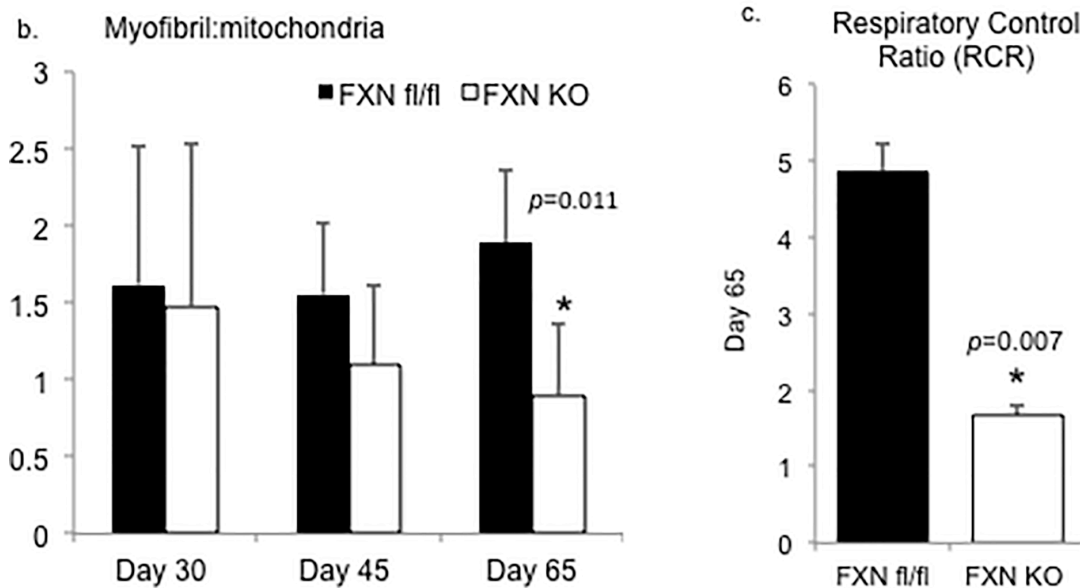
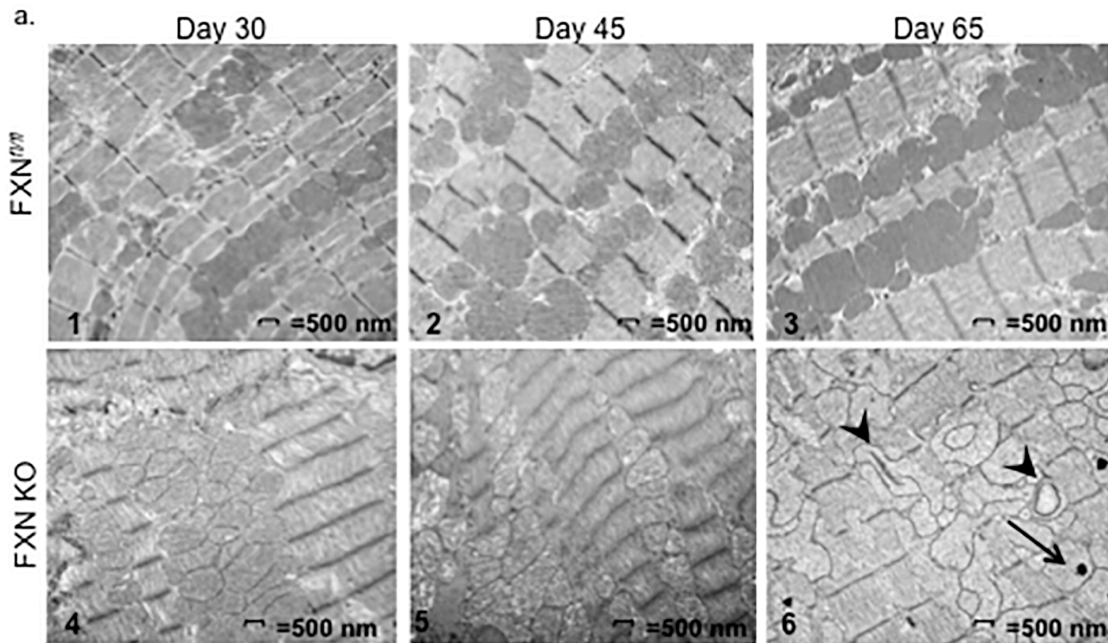


Figure 2-4. Abnormal cardiac mitochondria ultrastructure is accompanied by respiratory inhibition in FXN KO hearts. (a) Representative images from electron micrographs of cardiomyocytes viewed at 11,000x. Mitochondrial ultrastructure abnormalities were apparent in FXN KO sections and progressed from days 30 to 65. Findings included matrix density loss, mitochondrial-to-sarcomere disarrangement, and accumulation and clumping of mitochondria. FXN KO day 65 mitochondria demonstrate cristae collapse and dissolution, and hyperdense inclusions. Arrowhead = collapsed cristae; arrow = electron-dense intramitochondrial inclusions. (b) Myofibril:mitochondria area ratios were significantly decreased at day 65 in FXN KO compared to controls (n=3-8 micrographs per group). (c) Mitochondrial functional assays demonstrated significantly decreased respiratory control ratios in FXN KO (pooled mitochondria from n=8-12 hearts) compared to controls (pooled mitochondria from n=4-6 hearts).

(78.1±26.7%) was significantly higher than in control micrographs in which no abnormalities were detected ($p=0.002$) (Figure 2-4).

We next examined mitochondrial respiratory function at day 65. Respiratory control ratios (RCR) in FXN KO cardiac mitochondria (1.67 ± 0.12) were significantly decreased compared to controls (4.86 ± 0.37) ($p<0.001$) when measured by Clark Oxygen electrodes using complex I substrates glutamate and malate (2-4).

FXN KO hearts exhibit features of maladaptive ventricular remodeling

Consolidated areas of fibrotic infiltration of the heart are widespread in FXN KO mouse hearts at day 65 (Figure 2-5), similar to previous reports (79). By measuring the percent of collagen detected in ventricular tissue on stained micrographs, we demonstrate that FXN KO mice have more than a 1.5 times increase in fibrotic involvement of ventricular tissue compared to controls (FXN KO = 9.1% vs. control 4.9%, $p=0.002$) (Figure 2-5). We did not find a significant increase in amount of collagen in the FXN KO hearts compared to controls at days 30 or 45 on histological examination. FXN KO hearts at day 65 also display diffuse cardiomyocyte degeneration, indicated by the presence of vacuolation on light microscopy (Figure 2-5). Degenerating cardiomyocytes were not detectable at earlier ages (data not shown).

Loss of FXN in the heart leads to cardiac steatosis and cold intolerance

Ventricular tissue of FXN KO at day 65 demonstrated a combined pattern of macro- and microsteatosis in cardiomyocytes (Figure 2-6), providing direct evidence of a defect in fat metabolism or utilization in these hearts.

Because mice with loss of MCAD, or VLCAD in the heart quickly become hypothermic when exposed to cold environment and die (84, 85), and, similarly, ablation of SIRT3 leads to cold intolerance (82), we predicted that the conditional FXN KO would be unable to maintain its core body temperature when exposed to a cold stress. Mice were fasted for 6 hours then placed in a cold room at 4°C with core body temperature monitoring every 30 minutes, for a total period of 180 minutes. Indeed, we found that cold exposure lead to a precipitous drop in body temperature and significantly decreased survival rate in the FXN KO animals compared to controls (Figure 2-6). The majority of the FXN KO animals expired or became moribund with body temperatures <19°C (at which time animals were euthanized for humane reasons) prior to cessation of the three hour time period (Figure 2-6). Both controls and FRDA mice were observed to be shivering with exposure to cold.

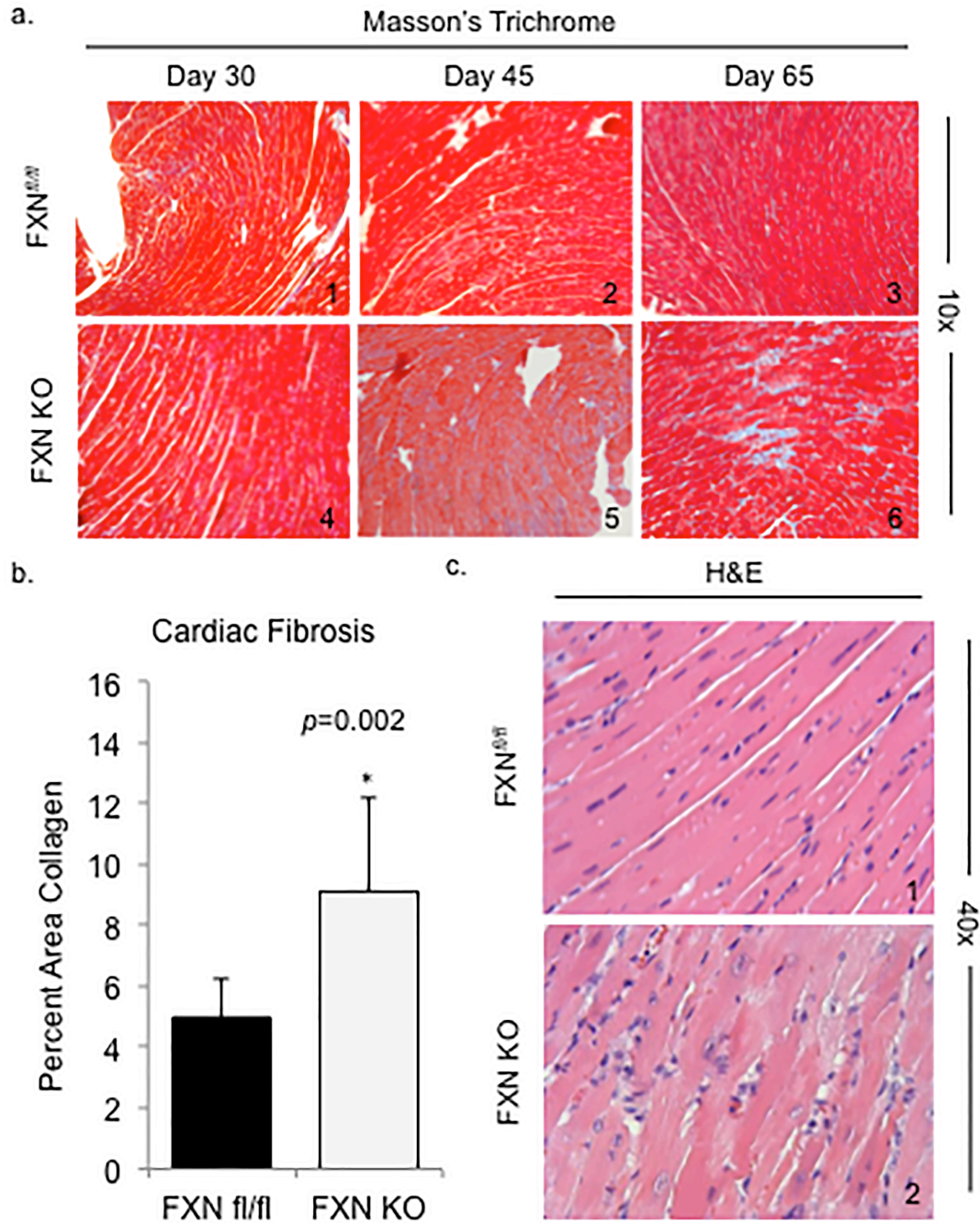


Figure 2-5. FXN KO hearts exhibit features of maladaptive ventricular remodeling. (a) Cardiac fibrosis is progressive in the FXN KO heart. Ventricular tissue was stained using Masson's Trichrome to detect blue-staining fibrous tissue. (b) Percent area collagen was significantly increased in FXN KO hearts at postnatal day 65 compared to controls. (c) Evidence of cardiomyocyte degeneration in the FXN KO at day 65 is demonstrated by vacuolation on H&E staining.

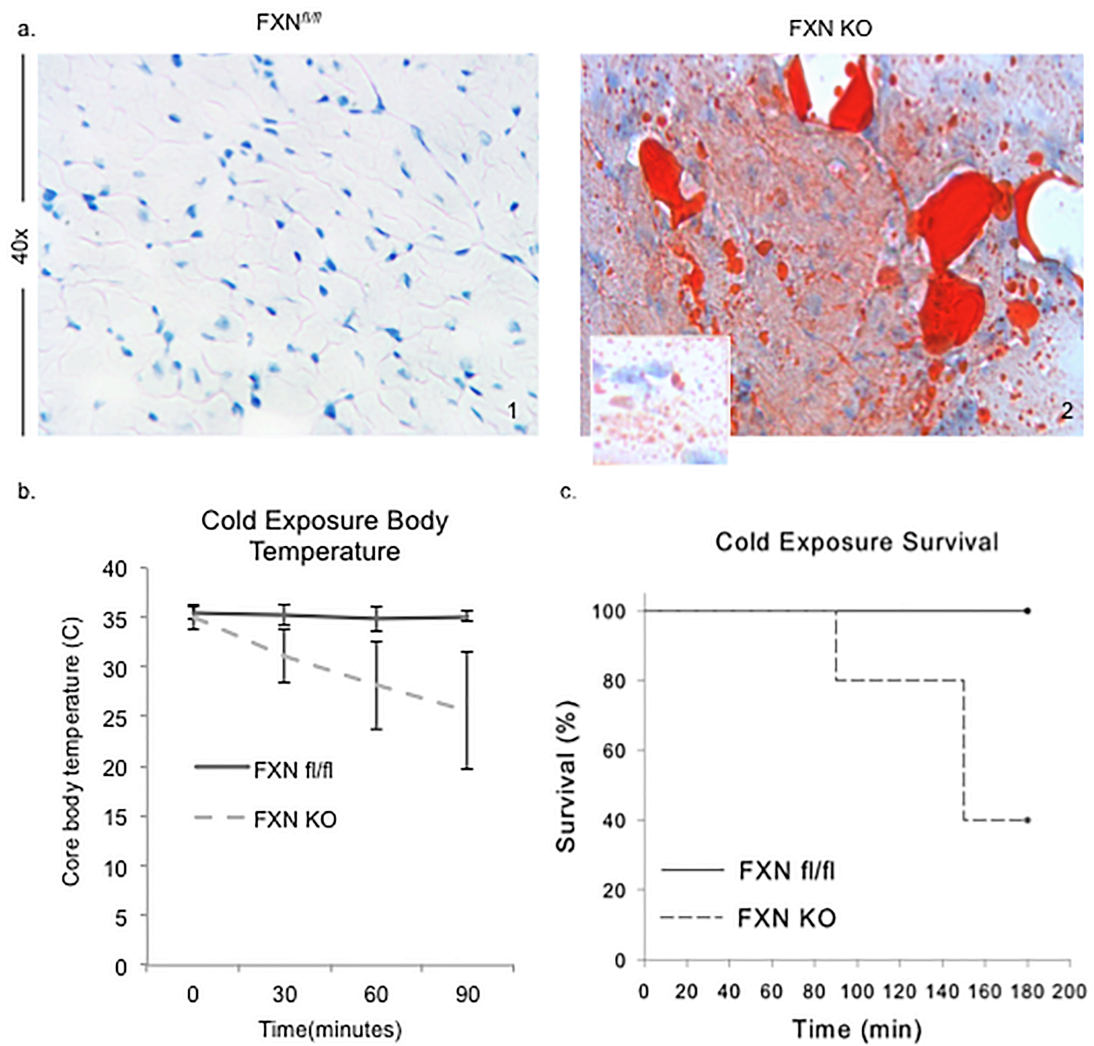


Figure 2-6. Loss of FXN in the heart leads to cardiac steatosis and cold intolerance. (a) FXN KO hearts demonstrate lipid accumulation in their hearts on Oil Red O staining. (b) Mice were subjected to a 6-hour fast after which they were placed in 4°C room for 3 hours with core body temperature monitoring. (c) FXN KO mice were unable to maintain core body temperature upon cold exposure and suffered significantly increased cold-related mortality rates compared to controls.

Discussion

This study is the first to document the progression of lysine-acetylated proteins and to demonstrate a correlation between acetylation and cardiac function in the heart of the conditional FXN KO mouse model of FRDA heart disease. We have characterized the early stages of cardiomyopathy in this important mitochondrial disease and followed its evolution to late-stage heart failure using an established animal model, that which mirrors that of the FRDA human heart disease. We conclude that protein lysine acetylation increases in a temporally progressive pattern and that there is a strong negative correlation between level of acetylation in the heart and global heart function: as acetylation increases, ejection fraction and fractional shortening decrease.

We found that abnormal post-translational modification of key metabolic enzymes has occurred prior to detectable impairment in heart function in the FXN KO. Acetylation is increased at day 30 and continues to progress over time. The first notable abnormal traits on cardiac pathophysiology occur at 45 days of age, with thickening of the left ventricular wall and diastolic dysfunction. As acetylation progresses, heart function continues to decline and demonstrates features of decompensated left ventricular dilation, decreased ejection fraction and fractional shortening, consistent with systolic heart failure. These results suggest that targeting acetylation early would provide the best chance to halt or slow progression of FRDA heart disease. Modifying acetylation only after detectable cardiac dysfunction occurs may miss the opportunity to prevent irreversible hemodynamic changes in the FXN KO heart that leads to heart failure.

Loss of SIRT3 in other murine models results in maladaptive ventricular remodeling in response to stress (42), abnormalities in lipid metabolism, and reduced tolerance to cold exposure (82). We found similar outcomes in the FXN KO, which has dysfunctional SIRT3 activity. This implies that loss of function of SIRT3 in the FXN KO heart and resultant hyper-acetylation of SIRT3 target proteins plays a major role in the pathologic processes of FRDA mitochondrial heart

disease. The absence of FXN in the heart, which has an established role in manufacturing of Fe-S cluster subunits needed for enzymes vital to oxidative metabolism, is, in and of itself, a major insult to the cardiomyocyte cellular milieu (86). The conditional FXN KO model thereby acts as a “stressed heart” model to examine the role of acetylation in heart disease and failure. This is supported by our observation that changes seen in the FXN KO are more robust, with an earlier age at onset, than those seen in models of SIRT3 loss alone. SIRT3 activity is impaired in FRDA hearts likely due to the decreased bioavailability of NAD^+ and to oxidative damage of SIRT3 (76). The findings in this study can be applied to other models of heart disease and failure. Many cardiac diseases with abnormal metabolism and energy homeostasis are liable to result in impaired SIRT3 activity in a manner similar to the FXN KO model, leading to abnormal mitochondrial protein acetylation in the heart and impaired cardiac function. Such heart disease candidates include inherited mitochondrial cardiomyopathies, diabetic and metabolic syndrome heart disease, acquired cardiac hypertrophy, age-related and ischemic heart disease, and heart failure (42, 71). For example, the ischemic heart results in a shift in redox state with accumulation of NADH (87), mirroring the consequential disturbance in energy equivalents in the FRDA heart.

More studies are needed in order to determine a causative role of abnormal acetylation in leading to impairment of hearts with FXN loss. For instance, it would be of great interest to determine whether normalizing the NAD^+/NADH ratio in the FXN KO heart would stimulate SIRT3 function, recover activity of targeted metabolic enzymes, and improve measured cardiac outcome. Recent work has shown that exogenous treatment with NAD^+ precursors can increase NAD^+ levels in mitochondria, reduce protein acetylation, and activate sirtuins (58, 59). Together with our findings that mitochondrial protein acetylation impairs heart function, this represents an attractive therapeutic potential for pharmacological modulation of protein lysine acetylation to improve cardiac metabolism and physiologic function and prevent unremitting progressive heart disease.

One limitation of this study may be that the MCK promoter used to drive Cre expression in this model is expressed in all sarcomeric tissues, including skeletal muscle. It is not expected that loss of FXN in skeletal muscle would significantly alter cardiac function in this study. Indeed, in patients with FRDA, and in the original report of this mouse model (79), there is not an identified skeletal muscle phenotype. Using the cardiac-specific alpha myosin heavy chain promoter (α -MHC) would address this limitation. However, we determined that the MCK promoter was the logical choice for these experiments both because the α -MHC has also been noted to be cardio-toxic under certain conditions (88), and we wanted to avoid this as a confounding variable, and because the MCK-Cre transgene has been used extensively in our lab and others' to generate the FXN KO mouse (76, 79).

In conclusion, we demonstrate a close relationship between mitochondrial protein acetylation, cardiac dysfunction and metabolic disruption in a model of FRDA hypertrophic cardiomyopathy. Our results suggest that abnormal acetylation contributes to the pathophysiology of heart disease in FRDA and may represent a therapeutic target for early intervention.

Methods

Mouse breeding and genotyping. This study was approved by the Institutional Animal Care and Use Committee of Indiana University. We used site-specific Cre-lox recombination to carry out gene deletions of interest. We used FXN^{f/f} mice to create FXN KO mice that were homozygous for heart and skeletal muscle deletion of FXN (MCK-Cre:FXN KO), as previously published (79). Data was collected from males at postnatal days 30(\pm 5), 45(\pm 4), and/or 65(\pm 5). Controls were age- and sex-matched healthy littermates (FXN^{f/f}).

Echocardiography (ECHO). Transthoracic ECHO images were obtained using a VisualSonics® 2100 ultrasound machine for small animal imaging and MS400 transducer (Fujifilm VisualSonics, Inc., Toronto, Canada). Functional parameters of the left ventricle and outflow tracts were measured using standard assessment techniques. Relative wall thickness (RWT) was calculated by $(2 * LVPWd) / LVIDd$.

Cardiac Catheterization. A 1.2 F catheter (Scisense, Transonic Systems Inc.) was inserted into the right carotid artery and advanced retrograde into the left ventricle. The Advantage system (Scisense, Transonic Systems Inc.) was used to acquire pressure, admittance, phase shift, and amplitude, and real time pressure-volume data was displayed and analyzed using Labscribe 2 (iWorx, Dover, NH).

Cold stress. This experiment was modeled after similar studies (84, 85). 65 day old FXN KO (n=5) and FXN^{*fl/fl*} (n=6) were selected for cold exposure. Mice were deprived of food for 6 hours prior to onset of study and for the duration of experiment. A baseline rectal temperature was taken prior to placement in 4°C cold room and then every 30 minutes thereafter for a total of 3 hours. A study was terminated for humane reasons if core body temperature reached 19°C or less.

Histology. Ventricular tissue selected for histology was fixed in 10% formalin and paraffin embedded. Histological analysis included hematoxylin and eosin (H&E) and Masson's Trichrome to detect collagen as a measure of fibrosis. Collagen quantification was performed using ImageJ (IJ1.46) to measure percent area of tissue positively stained for collagen. Three to five 20x digital micrographs were obtained from each tissue section that underwent quantification studies.

Electron Microscopy (EM). Ventricular tissue selected for electron microscopy was fixed in 2.5% glutaraldehyde and underwent sectioning and uranyl acetate staining by the Electron Microscopy

Center of Indiana University School of Medicine. At least 3 separate sections from each animal strain were selected for quantification analysis. Quantification methods were similar to methods used in our previous work (83). Abnormal mitochondria were identified as those containing electron-dense inclusions, cristae loss or dissolution, and/or collapsed or condensed cristae. Mitochondria and myofibril area was measured using ImageJ (IJ1.46).

Isolation of Cardiac Mitochondria. Mitochondrial isolation followed the method described in our previous work (76). Freshly harvested hearts were submerged in ice-cold mitochondrial isolation buffer. Heart tissue was weighed, homogenized, and then subjected to differential centrifugation. The mitochondrial pellet was resuspended in the appropriate buffer and used immediately for respiration assay or western blotting, or flash frozen for later analysis.

Mitochondrial respiration. Mitochondrial isolates designated for use in respiration assays were resuspended in mitochondrial respiration buffer. A total of 2-3 mouse heart mitochondria were combined for each run, with n=4-6 pooled heart mitochondria assayed for controls and n=8-12 pooled heart mitochondria assayed for FXN KO. A Clark-oxygen electrode was used for respiration assays. Glutamate and malate were used as a substrate for all assays.

Antibodies and Western Blotting. Primary antibodies included anti-acetyl-lysine (Cell Signaling #9441), anti-SIRT3 (Cell Signaling #5490), anti-SOD2 (acetyl K68) (Abcam ab137037), anti-SOD2 (Cell Signaling #13141), anti-VDAC (Cell Signaling #4866), anti-GAPDH (Cell Signaling #5174), anti-FXN (generous gift of Grazia Isaya, Mayo Clinic, Rochester MN), anti-LCAD (Abcam ab196655) and to the electron transport chain complexes: anti-CI-NDUFA9 (Abcam ab14713), anti-CII-SDHB (Abcam ab14714) and anti-CIII-UQCRCFS1 (Abcam ab14746). Band intensities were measured using ImageJ (IJ1.46). To determine correlation between acetylation

and heart function, relative density of acetylation for n=3 western blot images was normalized to day 30 controls and averages for each group were used for correlation calculation.

Statistics. All calculations, analyses and graphs were performed using SigmaPlot (Systat Software, Inc.). Two groups were compared using a two-tailed student's t test for samples with equal variance. Final data are presented as mean (\pm SD). Alpha was set at 0.05 and power at 0.800. A *p*-value of <0.05 was considered statistically significant.

CHAPTER 3

LOSS OF SIRTUIN 3 ACCELERATES HEART FAILURE IN A MURINE MODEL OF FRIEDREICH'S ATAXIA MITOCHONDRIAL HEART DISEASE

Introduction

The heart disease in Friedreich's Ataxia (FRDA) results from inherited deficiency of frataxin (FXN), a mitochondrial protein important in energy homeostasis. FXN is a highly conserved mitochondrial matrix protein that functions in iron-sulfur cluster assembly, which is integral to mitochondrial metabolic machinery (73). Reduced expression of FXN in FRDA causes impaired energy generation, decreased NAD^+/NADH ratio, and increased oxidative stress (9, 74, 75). In addition to ataxia, patients almost universally exhibit cardiac complications, which are characterized by arrhythmias, hypertrophic cardiomyopathy and heart failure. Heart disease is responsible for the majority of death in FRDA (48). FRDA is a relentlessly progressive disease for which there is no cure.

Mitochondrial protein acetylation is a post-translational protein modification that functions as a key regulator of cardiac metabolism and appears to play an important role in heart disease (89-92). SIRT3 is responsible for regulating mitochondrial protein lysine acetylation in response to cellular energy status by NAD^+ -dependent deacetylation of its target proteins, which are typically activated in response to deacetylation (10-12). SIRT3 targets include metabolically active enzymes, such as those of fatty acid oxidation, pyruvate and acetate metabolism, and the electron transport chain (6, 16-19, 21-24, 93), as well as the mitochondrial reactive oxygen species scavenger, superoxide dismutase 2 (SOD2) (34-36). In the heart, SIRT3 provides protection from a variety of stressors, such as ischemia and ischemia/reperfusion injury and

mechanical stress (39-41) and has been shown to attenuate lipotoxic cardiomyopathy and pressure-overload hypertrophy (42-45).

In a conditional murine model of FRDA cardiomyopathy, mitochondrial proteins have increased acetylation and decreased activity of SIRT3 (9). This reduction in SIRT3 activity is likely due to insufficient NAD⁺ bioavailability as a result of dysfunctional energy metabolism by the FXN-depleted mitochondria. More recently, we demonstrated a temporally progressive level of mitochondrial acetylation in a conditional knockout model of FRDA heart failure and a strong, negative correlation between level of acetylation and cardiac function in these hearts (62).

Recent work has shown that exogenous treatment with NAD⁺ precursors can increase NAD⁺ levels in mitochondria to activate sirtuins and reduce protein acetylation (58, 59). NAD⁺ repletion has been shown, specifically, to increase SIRT3 activity and provide protection from cardiac injury (60). This represents an attractive therapeutic potential for pharmacological modulation of protein lysine acetylation to improve cardiac metabolism and physiologic function.

We propose that abnormal acetylation impairs heart function in the FRDA heart. To test this hypothesis, we modified acetylation in the FRDA murine model heart by ablating SIRT3 gene expression altogether to create a double knockout mouse (FXN/SIRT3 DKO) and determined whether this led to changes at the cellular and molecular level to exhibit changes in cardiac pathophysiology when compared to FRDA and healthy controls. We also tested the hypothesis that NR therapy would normalize the NAD⁺/NADH ratio in the FXN KO heart, stimulate SIRT3 function to reduce acetylation levels and recover activity of targeted metabolic enzymes, and would result in improvement in measured cardiac outcome.

Results

Subcellular location of protein acetylation

SIRT3 is established as the major deacetylase in mitochondria (70), however, the subcellular location of active SIRT3 in other compartments remains controversial (94). Because FRDA arises from a specific mitochondrial defect that leads to inactivation of mitochondrial SIRT3 and increased mitochondrial protein acetylation (9, 62), we suspected that the majority of protein acetylation in the FXN KO heart would be localized to the mitochondria. To test this hypothesis, we performed cellular fractionation to separate the mitochondria from cytosolic cellular components and probed each fraction for lysine acetylation. We were surprised to find that ablating SIRT3 in the heart results in a robust increase in both cytosolic and mitochondrial protein lysine acetylation (Figure 3-1). In fact, the majority of acetylated proteins are contained in the cytosolic compartment in the control, FXN KO and SIRT3 KO hearts, with the exception being the FXN/SIRT3 DKO. Our findings indicate that SIRT3 is important in regulating both cytosolic and mitochondrial lysine acetylation. We were also interested to detect SIRT3 in both cytosol and mitochondria. The precise cellular location of SIRT3 remains controversial. Some researchers have reported SIRT3 in multiple cellular compartments, including the nucleus, cytosol and mitochondria (95, 96), while others have documented exclusive mitochondrial SIRT3 expression (10, 97).

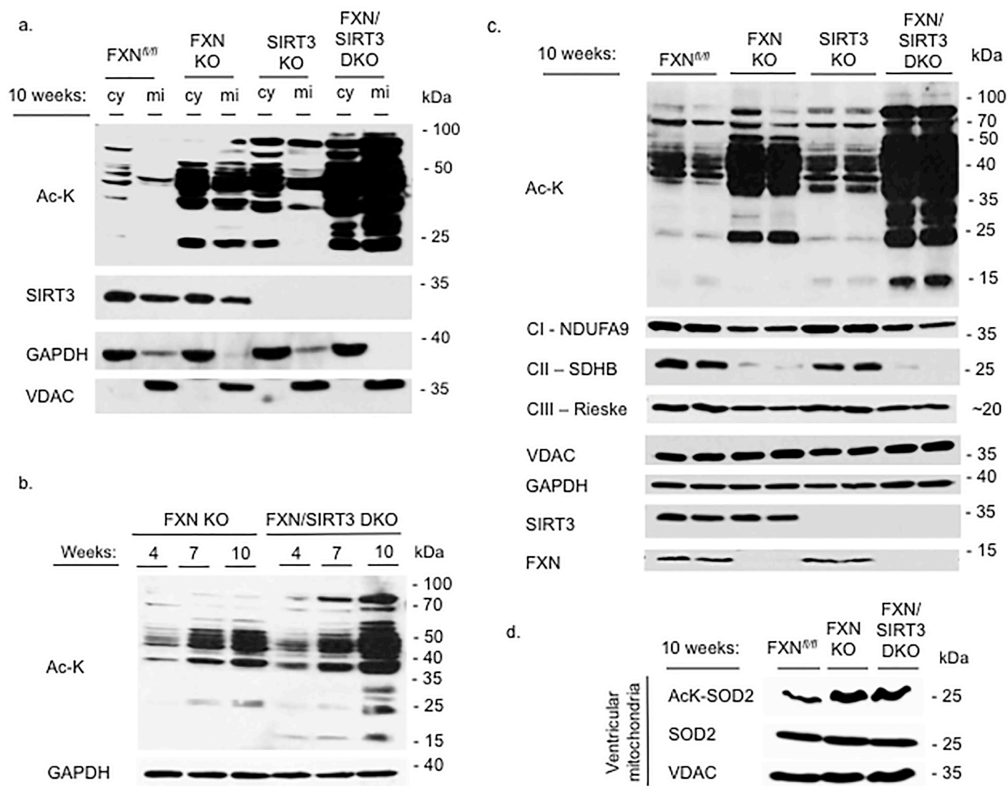


Figure 3-1. Acetylation is increased in FXN/SIRT3 DKO hearts. Whole cell preparations or mitochondrial isolates from ventricular tissue were probed for proteins of interest as indicated. (a) comparison of acetylation between cytosolic and mitochondrial compartments. (b) FXN/SIRT3 DKO acetylation compared to FXN KO mice at weeks 4, 7 and 10 shows increased acetylation at each time point in the FXN/SIRT3 DKO hearts. (c) Neither acetylation nor SIRT3 ablation affect the expression of electron transport chain proteins. (d) Proteins from isolated cardiac mitochondria were probed for SOD2 acetylated at Lys-68 (AcK-SOD2) to demonstrate increased acetylation of a specific SIRT3 target protein in FXN KO and FXN/SIRT3 DKO mitochondria.

Acetylation in the FXN KO heart increases in the absence of SIRT3 expression

Acetylation increases in conditional FXN KO hearts with age and correlates with declining heart function (62). Hearts in FXN/SIRT3 DKO mice demonstrate a robust increase in protein acetylation compared to age-matched FXN KO hearts, and follow a temporally progressive acetylation in a manner similar to FXN KO hearts (Figure 3-1).

We used the acetylation state of a specific mitochondrial target of SIRT3 as readout for SIRT3 deacetylase activity. To confirm that SIRT3 deacetylase activity is absent in the FXN KO and FXN/SIRT3 DKO hearts, we probed for acetylation of SOD2, which is a known SIRT3 protein target. SOD2 acts to destroy superoxide radicals and is inhibited when acetylated at lysine 68. SIRT3 reverses SOD2 acetylation (34, 81). We detected increased acetylated SOD2 in both FXN KO and FXN/SIRT3 DKO cardiac mitochondria at similar levels compared to controls (79.9% and 78.7% increase, respectively) (Figure 3-1). This finding is consistent with the absence of SIRT3 deacetylase activity, leading to SOD2 inhibition in these hearts.

We next investigated the relationship between acetylation and expression of essential mitochondrial electron transport proteins in FXN KO and FXN/SIRT3 DKO hearts. We know that the expression of enzymes utilizing Fe-S cluster components decreases progressively in FXN KO hearts (62) which, in itself, impairs energy generation capacity. Because SIRT3 acts in a post-translational manner and has not been shown to affect protein expression, we expected that deletion of SIRT3 would not affect the expression levels of essential mitochondrial electron transport proteins. Therefore, in order to verify that differences detected in the knockout hearts on cellular, molecular or functional levels result from loss of SIRT3-induced post-translational modifications of metabolically active proteins, and not from changes in SIRT3 target protein expression, we compared expression levels of ETC complexes in FXN KO and FXN/SIRT3 DKO

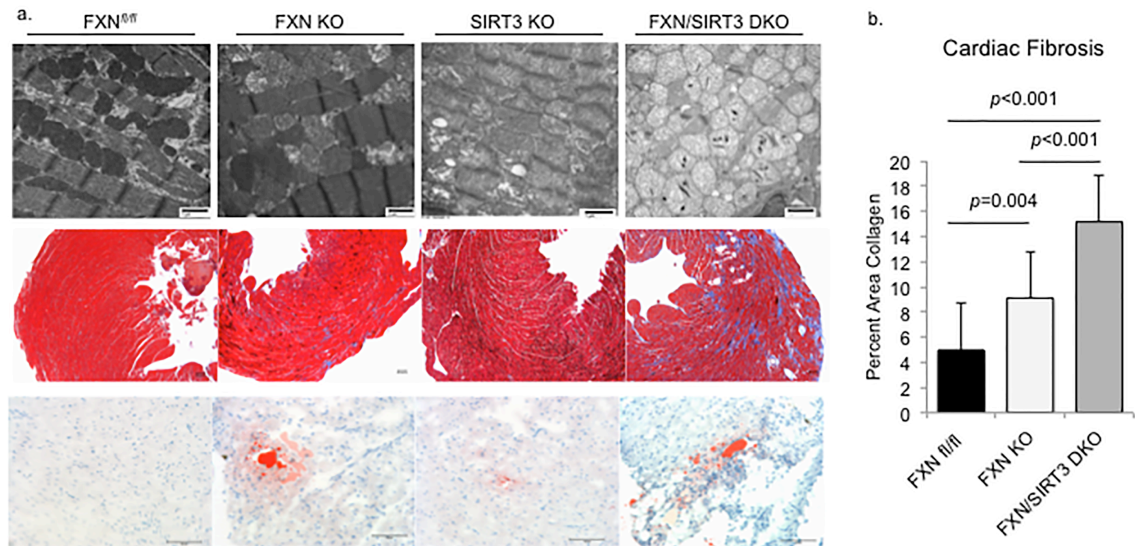


Figure 3-2. Loss of SIRT3 increases cardiac fibrosis in the FXN KO heart. (a) Ventricular tissue underwent sectioning and staining for electron microscopy to examine mitochondrial ultrastructure (top panel). Ventricular tissue was stained with Masson's trichrome to detect blue staining fibrosis (middle panel) or Oil Red O to detect lipids (bottom panel). (b) Cardiac fibrosis is significantly increased in FXN/SIRT3 DKO hearts.

mice at week 10 with matched FXN^{fl/fl} and SIRT3 KO controls to confirm that loss of FXN, and not loss of SIRT3 or increased protein acetylation, was responsible for the observed decrease in transport chain protein expression. As expected, (9, 62, 73), the expression of electron transport chain complex subunits CI-NDUFA9, CII-SDBH and CIII-Rieske is markedly diminished FXN KO hearts at 10 weeks of age, yet there were no differences in expression of electron transport chain subunits in the FXN KO compared to FXN/SIRT3 DKO at 10 weeks of age (Figure 3-1).

FXN KO and FXN/SIRT3 DKO hearts demonstrate abnormal cardiomyocyte mitochondria ultrastructure

We next asked whether deletion of SIRT3 in the FXN KO heart would lead to a structural impact on the mitochondria at the organelle level. There is progressive loss of normal mitochondrial ultrastructure in the FXN KO heart, which is associated with increasing levels of acetylation (62). We used electron microscopy to compare ventricular tissue of 10-week FXN KO to FXN/SIRT3 DKO and controls. Widespread pathologic changes were observed in the cardiomyocyte mitochondria of FXN KO and FXN/SIRT3 DKO (Figure 3-2). Mitochondrial ultrastructure changes include loss and collapse of cristae, disordered mitochondria-to-sarcomere arrangement, and extensive accumulation and stacking of mitochondria, in addition to widespread electron-dense inclusions. We also observed abnormalities in the SIRT3 KO heart mitochondria with generalized loss of cristae at 10 weeks of age.

To quantify the observed mitochondrial features in the FXN KO and FXN/SIRT3 DKO, we measured the ratio of myofibril-to-mitochondria area from micrographs, and determined the percentage of abnormal mitochondria (62, 98). The myofibril-to-mitochondria ratio was significantly decreased in FXN KO (0.901 ± 0.462) and FXN/SIRT3 DKO (0.771 ± 0.195) compared to controls (1.89 ± 0.471) ($p=0.013$), however, there was no significant difference between FXN KO ratio and FXN/SIRT3 DKO ratios ($p=0.661$) (Figure 3-2).

Deletion of SIRT3 in the FXN KO heart increases cardiac fibrosis

Fibrotic infiltration of the heart arises within a diverse array of cardiac pathologies, and typically is a response to injury of healthy myocardium by replacement with deposition of collagen fibers. Abnormal accumulation of fibrosis in the heart leads to ventricular wall stiffness,

perfusion defects and electrophysiologic dysfunction (99). Fibrosis is widely prevalent in FXN KO hearts as they age, as previously published (62). Here, we demonstrate that ventricular fibrosis is increased substantially in FXN/SIRT3 DKO hearts compared to FXN KO (Figure 3-2). Loss of SIRT3 expression in the FXN KO heart leads to more than a 1.5 times increase in fibrotic involvement of ventricular tissue as noted on histopathology (FXN KO = 9.1% vs. FXN/SIRT3 DKO = 15.2% tissue field area composed of collagen, $p < 0.001$).

Cardiac adiposity is known to be a marker of defective lipid metabolism in the heart and is associated with lipotoxic cardiomyopathy of diabetes, obesity-related heart disease and heart failure (100-103). We previously documented evidence of dysfunctional lipid metabolism in FXN KO hearts with the presence of cardiac steatosis (62). Here, we show similar areas of cardiac steatosis in the double knockout mouse heart (Figure 3-2). Mice with absence of SIRT3 expression develop excessive lipid accumulation in the heart compared to controls in response to pressure overload stress (42). We found that, at baseline, 10 week-old conditional SIRT3 KO mice develop areas of abnormal lipid accumulation in their hearts. This provides evidence that loss of myocardial SIRT3 alone is sufficient to cause steatosis in the heart at 10 weeks of age, even in the absence of external stressors.

Loss of SIRT3 increases protein acetylation and worsens heart failure in the FXN KO heart

We previously provided a detailed description of the progression from asymptomatic early-stage heart disease to end-stage heart failure in the FXN KO mouse. The FXN KO mouse heart is characterized by features that closely mirror the human FRDA heart disease such as early diastolic dysfunction and cardiac hypertrophy progressing rapidly to decompensated, dilated heart failure (62, 77). We established a strong negative correlation between heart function and level of cardiac mitochondrial protein acetylation, such that as acetylation levels increased, heart function

worsened (62). Considering the robust increase in mitochondrial protein acetylation in the double knockout heart, we were interested in determining what changes to pathophysiologic functional outcome would occur due to this increase.

Acetylated knockout hearts are hypertrophic with early diastolic dysfunction

Multiple anatomic parameters in the FXN KO and FXN/SIRT3 DKO mice are consistent with cardiac hypertrophy as early 7 weeks of age (Table 3-1). Week 7 FXN KO and FXN/SIRT3 DKO mice have thickened left ventricular posterior walls in diastole (LVPWd) (FXN KO = 0.838 ± 0.134 mm, FXN/SIRT3 DKO = 0.859 ± 0.168 mm), increased relative wall thickness (RWT) (FXN KO = 0.439 ± 0.085 ; FXN/SIRT3 DKO = 0.424 ± 0.076), and increased gross heart:body weight ratio (FXN KO = 5.58 ± 1.71 , FXN/SIRT3 DKO = 5.77 ± 1.04), compared to FXN^{fl/fl} controls (LVPWd = 0.643 ± 0.078 mm; RWT = 0.332 ± 0.050 ; heart:body weight = 4.40 ± 0.47). Knockout mice at week 7 also have increased ECHO-derived LV:body weight ratios (FXN KO = 5.17 ± 0.89 and FXN/SIRT3 DKO = 5.14 ± 1.93) compared to FXN^{fl/fl} mice (3.92 ± 0.69).

Diastolic dysfunction occurs early and precedes the onset of heart failure in the knockout models (Table 3-1). Both FXN KO and FXN/SIRT3 DKO mice demonstrate restrictive LV filling at 7 weeks of age, measured by increased mitral blood flow velocity ratio of *Early-to-Atrial* waves (E/A) on Doppler imaging (FXN KO = 2.36 ± 0.83 , and FXN/SIRT3 DKO = 2.82 ± 0.86 compared to FXN^{fl/fl} controls = 1.56 ± 0.22).

FXN KO and FXN/SIRT3 DKO hearts have persistent diastolic dysfunction with a transition to dilated cardiomyopathy.

Not surprisingly, both FXN KO and FXN/SIRT3 DKO mice demonstrate progressive cardiac dysfunction with relaxation abnormalities, cardiomegaly and dilated cardiomyopathy at 10 weeks of age (Table 3-1 and 3-2, Figures 3-3 and 3-4). Mitral blood flow velocity ratio (E/A) remains elevated at 10 weeks of age (FXN KO = 3.80 ± 1.45 ; FXN/SIRT3 DKO = 3.59 ± 1.02 , vs. FXN^{fl/fl} controls = 1.37 ± 0.15). Another marker of relaxation dysfunction, isovolumic relaxation time (IVRT), is increased at 10 weeks (FXN KO = 33.6 ± 4.2 msec; FXN/SIRT3 DKO = 35.3 ± 4.8 msec vs. FXN^{fl/fl} controls = 21.9 ± 2.5 msec). The presence of cardiomegaly is apparent at 10 weeks by ECHO-derived LV:body ratio, which is greater in both FXN/SIRT3 DKO (8.00 ± 2.82) and FXN KO mice (5.92 ± 1.08) compared to controls (3.47 ± 0.70). Left ventricle hypertrophy is also present with increased LVPWd in FXN KO (0.852 ± 0.23 mm) and FXN/SIRT3 (0.853 ± 0.23 mm) compared to controls (0.62 ± 0.13 mm).

Findings of LV dilatation are present in both knockout groups at 10 weeks of age. We found significant increases in LV internal diameter in diastole (LVIDd) in FXN KO (4.50 ± 0.598 mm) and FXN/SIRT3 DKO (5.06 ± 0.562 mm) compared to FXN^{fl/fl} (3.91 ± 0.141 mm). LV volume at end-diastole derived with ECHO, used here to estimate end diastolic volume (EDV), is increased as well in FXN KO and FXN/SIRT3 DKO mice ($94.7 \pm 29.7 \mu\text{l}$ and $123.4 \pm 31.5 \mu\text{l}$, respectively) compared to controls ($67.4 \pm 4.5 \mu\text{l}$). These findings are consistent with a transition from cardiac hypertrophy to dilated cardiomyopathy in the knockout hearts between 7 and 10 weeks of age.

Loss of SIRT3 in the FXN KO heart increases protein acetylation and worsens heart failure

Deletion of SIRT3 in the FXN KO mouse exacerbates heart failure. FXN/SIRT3 DKO animals demonstrate significantly depressed global contractile function compared to the FXN KO animals on ejection fraction (EF) (FXN KO = $26.6 \pm 10.4\%$; FXN/SIRT3 DKO = $12.7 \pm 10.3\%$, $p = 0.011$) and fractional shortening (FS) (FXN KO = $12.4 \pm 5.01\%$; FXN/SIRT3 DKO = $5.77 \pm 4.79\%$, $p=0.017$). This is consistent with our previous findings that the level of acetylation negatively correlates with heart function, and with the established role of SIRT3 protection in the heart.

Hypertrophic cardiomyopathy with conditional loss of SIRT3

Previous studies have reported cardiac hypertrophy in unconditional SIRT3 KO mice as early as 8 weeks of age, even in the absence of external stressors such as systemic pressure overload (25, 43). In order to confirm that conditional loss of SIRT3 in the heart, independent of FXN loss, would lead to similar findings of hypertrophy in non-stressed hearts at 10 weeks of age we compared the function of SIRT3 KO hearts to age-matched healthy SIRT3^{fl/fl} control littermates (Table 3-3). Indeed, the SIRT3 KO heart shows the beginning stages of hypertrophic remodeling at 10 weeks of age. SIRT3 KO hearts have significantly thicker posterior walls, LVPWd, compared to SIRT3^{fl/fl} (0.947 ± 0.105 vs. 0.807 ± 0.045 mm; $p=0.003$), as well as higher RWT (0.461 ± 0.053 vs. 0.395 ± 0.046 ; $p=0.015$). However, SIRT3 KO mice do not have increased LV:body weight (4.76 ± 0.61 vs. 4.62 ± 0.83 ; $p=0.683$) or heart:body weight compared to SIRT3^{fl/fl} (5.14 ± 0.22 vs. 5.07 ± 0.47 ; $p=0.697$).

Consistent with LV hypertrophy, SIRT3 KO have decreased end diastolic volume (EDV) and increased end diastolic pressure (EDP) compared to SIRT3^{fl/fl} at 10 weeks (SIRT3 KO =

30.15 ±9.28 uL vs. SIRT3^{fl/fl} = 46.40 ±9.92 uL, $p=0.006$; and SIRT3 KO = 11.24 ±4.20 vs. SIRT3^{fl/fl} = 5.66 ±3.14 mmHg, $p=0.030$, respectively). However, SIRT3 KO mice do not demonstrate significant diastolic abnormalities at this stage. Specifically, there are no differences compared to SIRT3^{fl/fl} in -dP/dt (-8,582 ±1,725 vs. -9,718 ±1,113 mmHg/sec; $p=0.132$) or E/A (1.57 ±0.21 vs. 1.65 ±0.24; $p=0.475$). IVRT in SIRT3 KO (22.25 ±1.46 msec) was longer compared to SIRT3^{fl/fl} (20.14 ±1.16 msec) but statistically similar to FXN^{fl/fl} (21.92 ±2.49 msec).

Contractile function is preserved in 10 week old mice with isolated loss of SIRT3. There are no differences in rate of contraction (+dP/dt) compared to SIRT3^{fl/fl} (11106 ±2679 vs. 13426 ±1939 mmHg/sec; $p=0.0640$) or global systolic function as measured by EF (56.7% ±11.55 vs. 57.41% ±12.10; $p=0.900$) and FS (29.85% ±7.68 vs. 30.40% ±8.29%; $p=0.8850$).

	Cardiac function measured by cardiac catheterization and echocardiography											
	4 weeks				7 weeks				10 weeks			
	F _{XN} ^{off} n = 7	F _{XN} KO n = 9	F _{XN} /SIRT3/DKO n = 5	ANOVA	F _{XN} ^{off} n = 7	F _{XN} KO n = 6	F _{XN} /SIRT3/DKO n = 6	ANOVA	F _{XN} ^{off} n = 7	F _{XN} KO n = 7	F _{XN} /SIRT3/DKO n = 0 ‡	ANOVA
CATH	AVG	AVG	AVG	p-value	AVG	AVG	AVG	p-value	AVG	AVG	AVG	p-value
HR (bpm)	605.3 ± 85.3	577.1 ± 44.6	733.2 ± 95.9	*0.004	671.4 ± 95.2	580.9 ± 81.4	585.6 ± 97.8	0.261	595.7 ± 77.1	643.3 ± 105.2		0.633
+dP/dt (mmHg/sec)	1011.5 ± 184.8	876.0 ± 96.2	1070.6 ± 246.3	0.114	1188.2 ± 192.8	687.5 ± 115.6	823.1 ± 109.6	*0.003	1080.9 ± 159.1	516.5 ± 110.1		*<0.001
-dP/dt (mmHg/sec)	-811.4 ± 106.7	-780.2 ± 81.7	-865.8 ± 150.7	0.388	-970.4 ± 79.9	-608.7 ± 13.78	-705.3 ± 117.6	*<0.001	-922.8 ± 89.1	-409.9 ± 104		*<0.001
maxPwr (mWatt)	107.5 ± 31.2	84.7 ± 14.5	116.0 ± 42.1	0.126	143.3 ± 32.1	67.5 ± 20.7	75.6 ± 15.99	*0.006	121.2 ± 31.5	37.3 ± 14.1		*<0.001
EDP (mmHg)	11.7 ± 4.5	11.0 ± 3.3	12.3 ± 3.3	0.806	10.9 ± 3.8	13.0 ± 5.7	11.8 ± 4.08	0.657	8.8 ± 3.0	10.0 ± 5.3		0.566
EDV (uL)	50.9 ± 6.6	45.7 ± 7.3	37.5 ± 8.3	*0.019	43.6 ± 12.2	48.2 ± 9.0	47.3 ± 11.22	0.750	53.4 ± 7.8	99.6 ± 15.2		*<0.001
ECHO	F _{XN} ^{off} n = 10	F _{XN} KO n = 10	F _{XN} /SIRT3/DKO n = 8	ANOVA	F _{XN} ^{off} n = 11	F _{XN} KO n = 11	F _{XN} /SIRT3/DKO n = 10	ANOVA	F _{XN} ^{off} n = 9	F _{XN} KO n = 9	F _{XN} /SIRT3/DKO n = 7	ANOVA
	AVG	AVG	AVG	p-value	AVG	AVG	AVG	p-value	AVG	AVG	AVG	p-value
EF (%)	55.0 ± 10.1	54.2 ± 7.3	52.1 ± 5.9	0.749	49.9 ± 13.7	46.3 ± 7.7	39.3 ± 12.3	0.121	47.7 ± 8.2	26.6 ± 10.4	12.7 ± 10.4	*<0.001
FS (%)	28.2 ± 6.4	27.6 ± 5.0	26.2 ± 3.6	0.720	25.6 ± 9.2	22.9 ± 4.4	19.1 ± 6.8	0.133	23.7 ± 4.9	12.4 ± 5.1	5.8 ± 4.8	*<0.001
LV Vol.d (uL)	55.0 ± 12.7	57.2 ± 15.5	57.6 ± 11.5	0.901	65.8 ± 11.1	64.9 ± 15.1	74.0 ± 17.5	0.314	67.4 ± 4.5	94.7 ± 29.7	123.4 ± 31.5	0.001
LVVIDd (mm)	3.6 ± 0.34	3.7 ± 0.42	3.7 ± 0.31	0.881	3.9 ± 0.26	3.9 ± 0.37	4.1 ± 0.42	0.348	3.9 ± 0.14	4.5 ± 0.60	5.1 ± 0.56	*0.001
LVPWd (mm)	0.61 ± 0.12	0.58 ± 0.14	0.7 ± 0.12	0.600	0.64 ± 0.08	0.84 ± 0.13	0.86 ± 0.17	*<0.001	0.62 ± 0.13	0.85 ± 0.23	0.85 ± 0.23	*0.039
RWT	0.35 ± 0.10	0.32 ± 0.08	0.35 ± 0.05	0.748	0.33 ± 0.05	0.44 ± 0.08	0.42 ± 0.08	*0.003	0.32 ± 0.07	0.39 ± 0.13	0.34 ± 0.11	0.408
E/A	1.7 ± 0.24	1.7 ± 0.21	2.0 ± 0.31	*0.046	1.5 ± 0.20	2.4 ± 0.87	2.8 ± 0.86	*0.001	1.4 ± 0.14	3.8 ± 1.5	3.6 ± 1.0	*0.002
IVRT (msec)	25.4 ± 3.5	23.6 ± 3.4	23.5 ± 2.9	0.376	23.4 ± 2.0	26.0 ± 3.8	23.7 ± 1.8	0.131	21.9 ± 2.5	33.6 ± 4.2	35.3 ± 4.8	*<0.001
LV:body (mg/g)	4.1 ± 1.4	4.5 ± 1.6	4.3 ± 0.84	0.855	3.9 ± 0.69	5.2 ± 0.89	5.1 ± 1.9	*0.032	3.5 ± 0.70	5.9 ± 1.1	8.0 ± 2.8	*<0.001

Table 3-1. Cardiac function measured by cardiac catheterization and echocardiography. * = statistical difference (p<0.05) in values among groups based on one-way ANOVA analysis. Each statistically significant group then underwent multiple pair-wise comparison procedures (see Table 3-2). ‡ = no values obtained for FXN/SIRT3 DKO due to their high mortality rate on cardiac catheterization procedure (see text). HR = heart rate; +dP/dt = rate of contraction; -dP/dt = rate of relaxation; maxPwr = power of left ventricle; EDP = end diastolic pressure; EDV = end diastolic volume; EF = ejection fraction; FS = fractional shortening; EDV; EDV = end diastolic volume; LVVIDd = left ventricular internal diameter, diastole; LVPWd = left ventricle posterior wall thickness diastole; E/A = ratio of early to atrial rate of mitral valve blood flow; IVRT = isovolumic relaxation time; LV:body = ratio of left ventricle to body mass.

Pairwise comparison for hemodynamics and ECHO				
vs.	FXN ^{fl/fl}	FXN ^{fl/fl}	FXN KO	
	FXN KO	FXN/SIRT3 DKO	FXN/SIRT3 DKO	
4	HR		**	
	EDV			
	EA†			
7	Age	*		
	+dP/dt	***	**	
	-dP/dt	***	***	
	maxPwr	***	***	
	LVPWd	***	**	
	RWT	**	**	
	EA	*	***	
10	LV:body	**	**	
	+dP/dt	***		
	-dP/dt	***		
	maxPwr	***		
	EDV	***		
	EF	***	***	*
	FS	**	***	*
	LV Vol d	*	*	
	LVIDd	*	***	
	LVPWd†			
	EA	***	***	
	IVRT	***	***	
LV:body	*	*		

p-value: *=<0.05, **=<0.01, ***=<0.001

Table 3-2. Pairwise comparison of heart function between groups. † Significance on ANOVA, but not on pairwise comparison analysis.

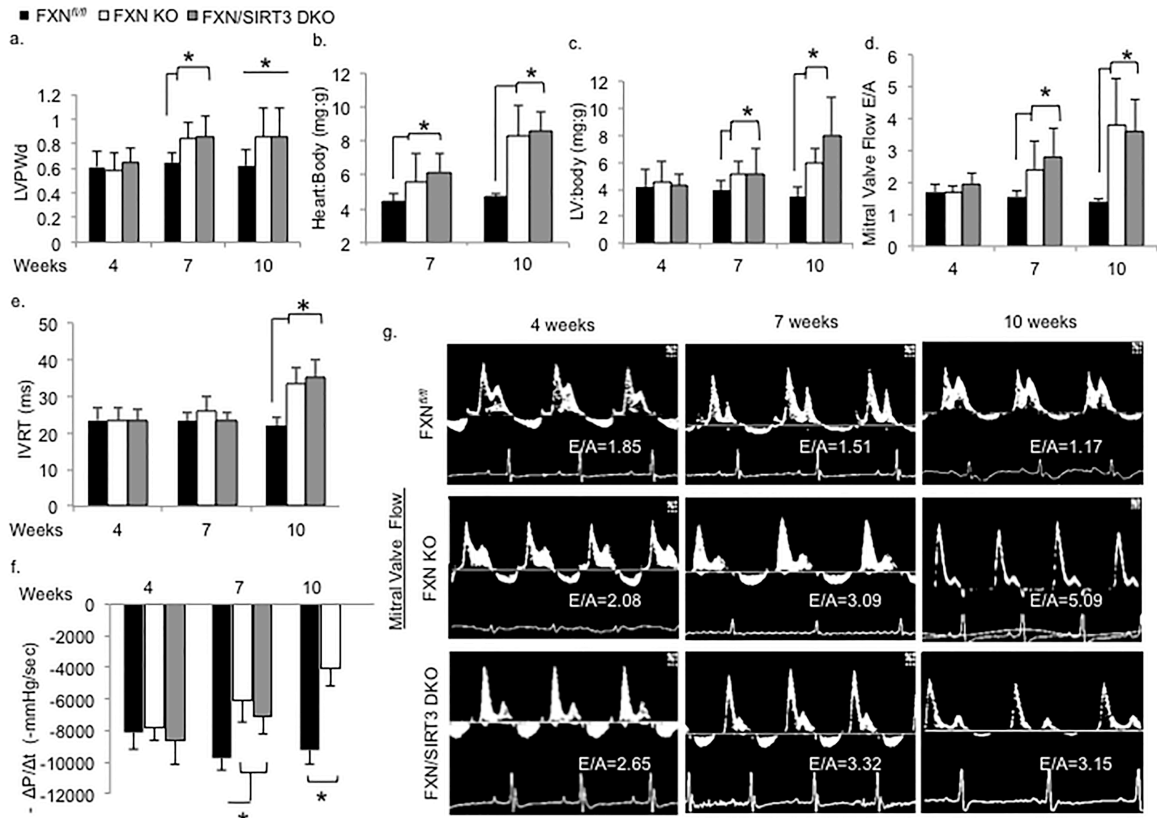


Figure 3-3. FXN KO and FXN/SIRT3 DKO heart function compared to controls. (a) FXN KO and FXN/SIRT3 DKO have cardiac hypertrophy (LVPWd) at weeks 7 and 10. (b) Total heart:body weight ratio is significantly increased at week 7 in FXN KO and FXN/SIRT3 DKO mice compared to FXN^{fl/fl} controls and progressively increases to week 10. (c) ECHO-derived LV:body mass ratios are elevated in week 10 FXN KO and FXN/SIRT3 DKO animals compared to FXN^{fl/fl} controls. (d) Relaxation abnormalities are apparent by increased E/A mitral flow ratios at weeks 7 and 10, and (e) isovolumic relaxation time (IVRT) at week 10 in FXN KO and FXN/SIRT3 DKO. (f) Left ventricle rate of relaxation ($-\Delta P/\Delta t$) is decreased compared to FXN^{fl/fl} controls in FXN KO and FXN/SIRT3 DKO animals on week 7, and on week 10 in FXN KO. (g) Mitral flow patterns demonstrate restrictive E/A flow ratio. LVPWd = left ventricle posterior wall diastolic thickness (mm); LV = left ventricle; E/A = ratio of the early (E) to late (A) ventricular filling velocities; IVRT = isovolumic relaxation time (ms); $-\Delta P/\Delta t$ = rate of relaxation ($-\Delta$ intra-ventricular pressure/ Δ time)(mmHg/sec). * $p < 0.05$; statistical significance between groups is indicated by lines connecting graph bars.

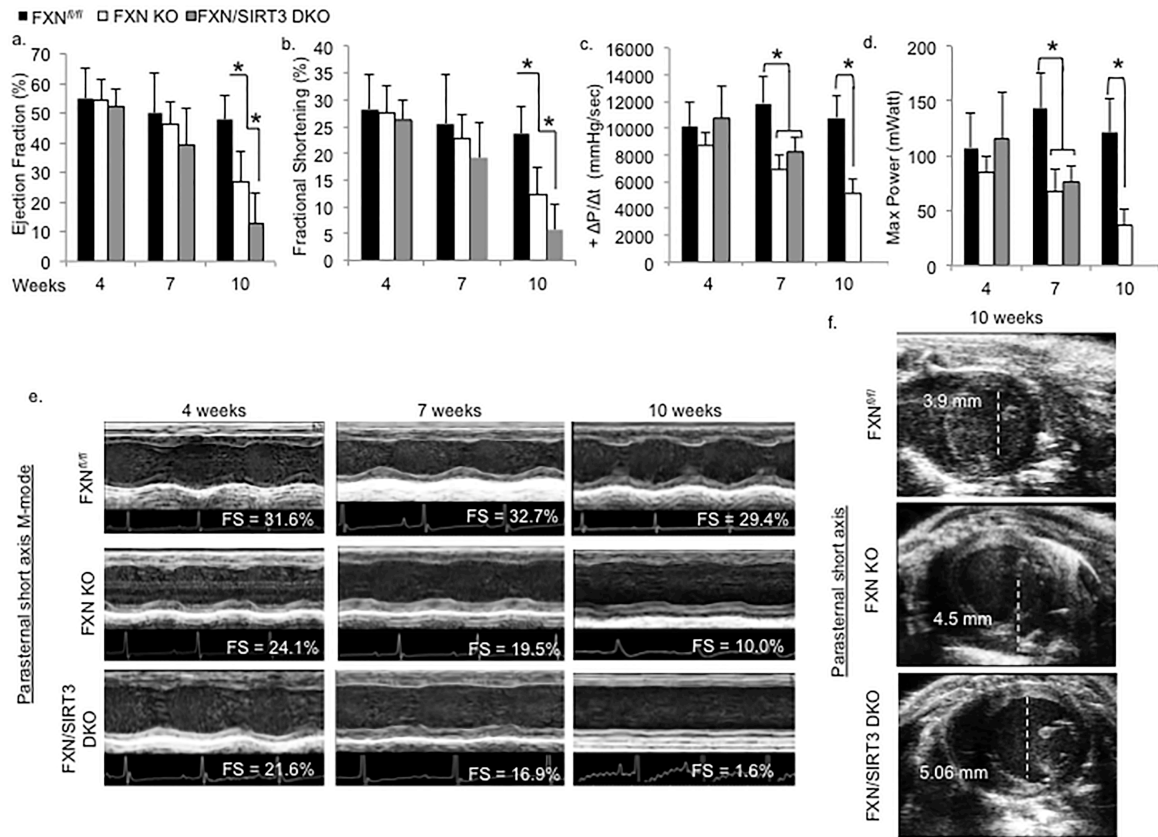


Figure 3-4. Loss of SIRT3 in FXN KO hearts exacerbates heart failure. (a) and (b) FXN/SIRT3 DKO demonstrate significantly depressed global contractility function compared to the FXN KO for EF ($p = 0.027$) and FS ($p = 0.037$). Catheterization data for FXN/SIRT3 DKO at 10 weeks is not present because the majority did not survive surgical catheterization (see text). (c) and (d) FXN/SIRT3 DKO and FXN KO had significantly slower rate of contraction (+dP/dt), and maxPower compared to FXN^{fl/fl} controls. (e) Representative echocardiographic parasternal short axis M-mode images demonstrate progressive impairment in left ventricular wall movement with decreased fractional shortening in FXN KO and FXN/SIRT3 DKO. (f) Parasternal axial images illustrate findings of hypertrophy with transition to dilated cardiomyopathy in FXN KO and FXN/SIRT3 DKO mice. +dP/dt = rate of contraction (+Δintra-ventricular pressure/Δtime)(mmHg/sec); $*=p<0.05$; statistical significance between groups is indicated by lines connecting graph bars.

Heart function of SIRT3 ^{fl/fl} and SIRT3 KO at 10 weeks			
	<u>SIRT3^{fl/fl}</u> n=9	<u>SIRT3 KO</u> n=7	
CATH	AVG	AVG	<i>p</i> -value
HR (bpm)	714.0 ±59.2	626.6 ±95.2	0.040
+dP/dt (mmHg/sec)	13426 ±1934	11105.88 ±2678.6	0.064
-dP/dt (mmHg/sec)	-9718 ±1113	-8582 ±1725	0.132
maxPwr (mWatt)	162.1 ±31.4	131.2 ±42.5	0.116
EDP (mmHg)	5.8 ±4.6	11.2 ±4.2	0.030
EDV (uL)	46.6 ±10.5	30.2 ±9.3	0.006
	<u>SIRT3^{fl/fl}</u> n=9	<u>SIRT3 KO</u> n=9	
ECHO	AVG	AVG	<i>p</i> -value
EF (%)	57.4 ±12.1	56.7 ±11.6	0.900
FS (%)	30.4 ±8.3	29.9 ±7.7	0.885
LV:body (mg:g)	4.6 ±0.83	4.8 ±0.61	0.683
LVIDd (mm)	4.1 ±0.42	4.1 ±0.33	0.983
LVPWd (mm)	0.81 ±0.05	0.95 ±0.11	0.003
RWT	0.40 ±0.05	0.46 ±0.05	0.015
EA	1.7 ±0.24	1.6 ±0.21	0.475
IVRT (msec)	20.1 ±1.2	22.3 ±1.5	0.020

Table 3-3. Heart function of SIRT3^{fl/fl} and SIRT3 KO at 10 weeks.

Loss of SIRT3 in the FXN KO heart increases stress-related mortality and rate of heart failure-associated weight loss

We next wanted to determine whether the changes observed at the cellular and organ level after deletion of SIRT3 in the FXN KO heart had a broader impact on physiologic outcomes, such as lifespan and growth pattern. Both the FXN KO and FXN/SIRT3 DKO had significantly foreshortened average lifespans. The mean age at death in the FXN KO mice (n=11) was 86.6 ± 9 days, and the FXN/SIRT3 DKO mice (n=10) was 84.9 ± 6 days (Figure 3-5). FXN^{fl/fl} (n=11) were followed for 120 days of postnatal life and no deaths occurred in this group within this period. We found no difference in non-stressed survival between FXN KO and FXN/SIRT3 DKO ($p=0.724$).

Weight loss begins at approximately 8 weeks of life in both FXN/SIRT3 DKO and FXN KO under unmodified conditions (Figure 3-5). Notably, the FXN/SIRT3 DKO mice lose weight at a significantly faster rate than the FXN KO animals (median rate (Δ mass (gm)/ Δ time (weeks))): FXN KO = -0.061 vs. FXN/SIRT3 DKO = -0.147, $p=0.003$). This accelerated weight loss may arise from a steeper decline in heart function in the FXN/SIRT3 DKO mice when compared with FXN KO mice. Consequently, the absence of SIRT3 expression in the double knockout appears to predispose the mice to a more aggressive onset of metabolic imbalance such as that seen in the wasting process of cardiac cachexia.

A final and remarkable physiologic outcome difference we found between the FXN KO and FXN/SIRT3 DKO mice was in their response to surgical intervention. The FXN/SIRT3 DKO

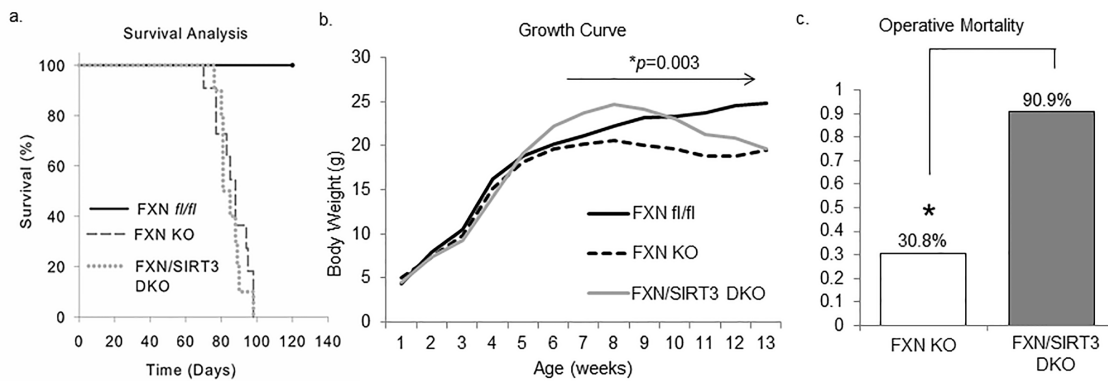


Figure 3-5. Loss of SIRT3 in FXN KO hearts increases operative mortality and accelerates weight loss. (a) There is no difference in overall non-stressed longevity between FXN KO (n=11) and FXN/SIRT3 DKO (n=10) ($p=0.474$). No deaths occurred in FXN^{fl/fl} (n=11). (b) FXN/SIRT3 DKO (n=10) peak at a higher body weight, but have an increased rate of weight loss from week 8 to 13 (Δ mass (g)/ Δ time (weeks)) compared to FXN KO (median rate FXN KO = -0.054 vs. FXN/SIRT3 DKO = -0.148, $p<0.001$). (c) Procedural mortality of FXN/SIRT3 DKO (n=12) is increased compared to FXN KO (n=17) at 65 days upon exposure to cardiac catheterization ($p=0.005$, 95% CI=-0.969 to -0.234).

mice are significantly more susceptible to death from surgical stress than FXN KO mice under the same operative conditions. Surgical mortality was markedly increased in the FXN/SIRT3 DKO (n=12) animals compared to FXN KO (n=17) (11 out of 12, or 90.9% vs. 4 out of 17, or 30.8%; $p=0.005$, 95% CI=-0.969 to -0.234) (Figure 3-5). This observation suggests that hyperacetylation in the heart leads to an increase in procedural risk and may have relevance in the perioperative clinical setting.

NAD⁺ replacement therapy with nicotinamide riboside increases mitochondrial protein acetylation and does not improve cardiac function in FXN KO mice

There is evidence that NAD⁺ repletion by oral supplementation with its precursor, nicotinamide riboside (NR), is effective at increasing mitochondrial NAD⁺ content, SIRT3 activity and improving mitochondrial function (58). Because SIRT3 is inactive in the FXN KO mouse heart likely secondary to decreased bioavailability of NAD⁺ from deficient energy production, we expected that recovering the NAD⁺ level in these cells would act to stimulate SIRT3 function. We tested the hypothesis that oral NR therapy would normalize lysine acetylation and improve cardiac performance in the FXN KO mice. We administered oral NR at 500 mg/kg/day to FXN KO mice (n=6) and healthy controls (n=6) from 4 weeks of age until 10 weeks of age.

NR supplementation was effective at increasing NAD⁺ content in the hearts of treated animals (Figure 3-6). We were surprised to find that FXN KO hearts demonstrated increased global mitochondrial protein lysine acetylation in response to exogenous treatment with NR. SIRT3 protein expression in mitochondria responded to NR therapy by increased expression. Despite the increase in mitochondrial SIRT3 expression, the acetylation state of SOD2, a known target of SIRT3 and our readout for SIRT3 activity in this study, remained similarly elevated in both treated and untreated FXN KO mice compared to controls. SOD2 did not increase to the extent that global acetylation increased, suggesting that up regulated SIRT3 expression was able to counteract a measure of the increased acetylation.

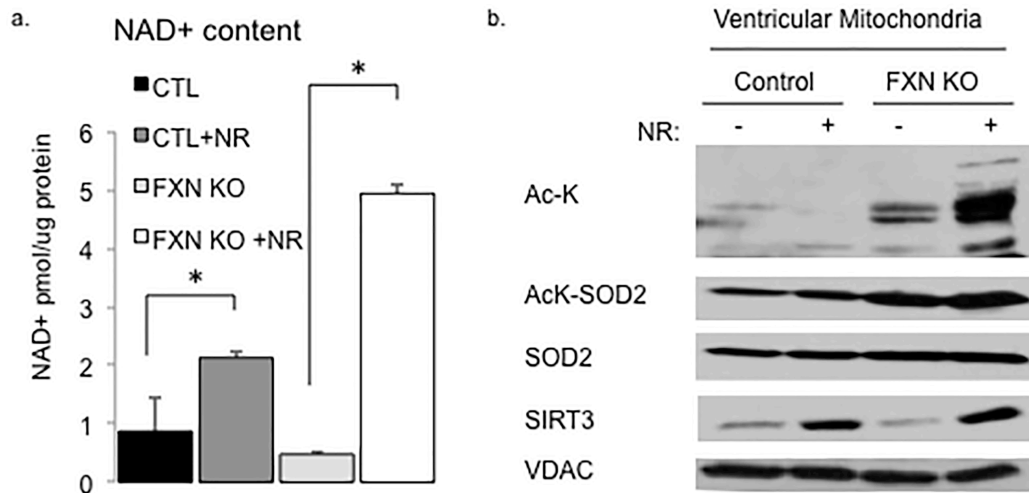


Figure 3-6. Mitochondrial protein acetylation increases in response to NR treatment in FXN KO mice. (a) Oral NR therapy is effective at significantly augmenting NAD⁺ content in FXN KO mice. (b) Mitochondrial protein lysine acetylation increases in NR-treated FXN KO hearts.

Cardiac function declined steadily with age in FXN KO animals and no significant improvements were noted after NR supplementation (Figure 3-7). Measurements included left ventricle thickness (LVPWd) (FXN KO -NR 0.85 ± 0.23 vs FXN KO +NR 0.78 ± 0.12 mm, $p=0.53$), ejection fraction (FXN KO -NR = 26.6 ± 9.7 vs. FXN KO +NR $30.6 \pm 13.5\%$, $p=0.53$), fractional shortening (FXN KO -NR 12.4 ± 4.7 vs. FXN KO +NR $14.5 \pm 6.7\%$, $p=0.51$) and rates of contraction (FXN KO -NR 5165 ± 1019 vs FXN KO +NR 4683 ± 760 mmHg/sec, $p=0.42$) and relaxation (FXN KO -NR -4099 ± 1022 vs. FXN KO +NR -3613 ± 807 mmHg/sec, $p=0.42$). Diffuse cardiac fibrosis was evident in FXN KO hearts at 10 weeks and there was no significant difference in fibrotic infiltration of the heart after NR therapy (Figure 3-7).

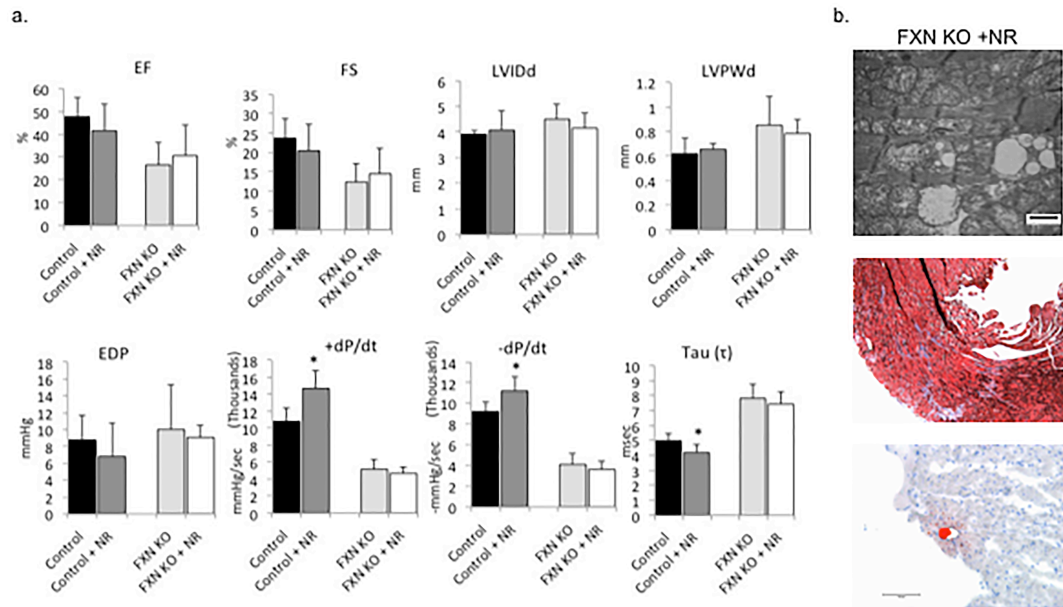


Figure 3-7. No improvement in functional heart outcome in FXN KO mice after treatment with NR. (a) Comparison of functional cardiac parameters after NR therapy. (b) Representative images from cardiac tissue of FXN KO animals treated with NR demonstrate abnormal mitochondrial morphology, intraventricular fibrosis, and cardiac steatosis (images top to botto). EF = ejection fraction; FS = fractional shortening; LVIDd = left ventricular internal diameter, diastole; LVPWd = left ventricular posterior wall diameter, diastole; EDP = end diastolic pressure; +dP/dt = rate of contraction; -dP/dt = rate of relaxation; Tau (weiss) = time constant of ventricular relaxation; n=5-7/group; *= $p < 0.05$.

TAT-FXN protein replacement therapy in FXN/SIRT3 DKO mice is sufficient to decrease, but not normalize, mitochondrial protein acetylation

We next asked whether replacement of FXN in the FXN/SIRT3 DKO mouse would be sufficient to rescue cardiac function. We have previously published data that fusion of FXN to a cell-penetrant peptide, transactivator of transcription (TAT), or TAT-FXN, is capable of replacing

Figure 3-8. FXN replacement in FXN/SIRT3 DKO mice reduces cardiac mitochondrial protein lysine acetylation. (a) FXN expression increases after TAT-FXN therapy. (b) Global cardiac whole cell and (c) mitochondrial lysine acetylation decreases in FXN/SIRT3 DKO hearts after treatment with TAT-FXN. (d) FXN/SIRT3 DKO mice treated with TAT-FXN exhibit persistent mitochondrial ultrastructure defects, fibrosis and cardiac steatosis (images left to right).

active FXN in FRDA cells and that TAT-FXN protein replacement therapy is effective at rescuing a severe phenotypic murine model of FRDA (98). We treated FXN/SIRT3 DKO mice (n=4) with twice weekly doses of TAT-FXN at 10 mg/kg body weight via intraperitoneal injection from 2 weeks of age to 10 weeks of age. At the end of therapy, we harvested heart tissue for further analysis to compare to untreated FXN/SIRT3 DKO mice.

We found that TAT-FXN therapy was sufficient to reduce mitochondrial protein acetylation levels in the FXN/SIRT3 DKO hearts (Figure 3-8). This finding suggests that even in the absence of SIRT3, the presence of functional FXN alone is sufficient to reduce the burden of

abnormally high levels of protein acetylation, possibly by allowing acetyl CoA intermediates to enter the TCA cycle via restoration of aconitase activity (98).

Despite therapy with TAT-FXN, immunohistochemical analysis and electron microscopy revealed cardiac fibrosis and steatosis, and widespread abnormalities in mitochondrial ultrastructure, similar to untreated animals. These results demonstrate that SIRT3 activity is necessary to fully rescue cardiac function in the FXN/SIRT3 DKO mouse model, and provides further evidence that SIRT3 plays an important role in FRDA cardiomyopathy. For instance, findings of myocardial lipid accumulation even after FXN replacement in the double knockout heart is not unsurprising considering others' reports that absence of SIRT3 leads to dysfunctional lipid metabolism. Inactive SIRT3 may, in fact, be a major contributor to disordered lipid metabolism in the FXN KO heart due to its inability to deacetylate and activate fatty acid enzymes.

Discussion

This study provides the first report that the conditional loss of SIRT3 expression in the heart of a model of known mitochondrial heart disease is sufficient to cause a robust increase in cardiac mitochondrial protein acetylation and worsen heart function. Removing expression of SIRT3 in the FXN KO heart dramatically increases protein acetylation and worsens the functional outcome of end-stage heart failure. Loss of SIRT3 in the FXN KO heart also exacerbates underlying cellular features of maladaptive ventricular remodeling, such as increased fibrosis of ventricular walls. Perhaps even more importantly, site-specific deletion of SIRT3 in our model leads to poorer physiologic outcomes, such as accelerated heart failure-associated wasting and increased mortality rate in response to surgical stress.

FXN has an established role in manufacturing of Fe-S cluster subunits needed for enzymes vital to oxidative metabolism. The FXN KO model thereby acts as a “stressed heart” model in which to study the influence of SIRT3 on the pathologic process of heart failure. SIRT3 activity is impaired in FRDA hearts likely due to the decreased bioavailability of NAD⁺ and to oxidative damage to SIRT3 (9). Other cardiac diseases with abnormal metabolism and energy homeostasis are expected to result in impaired SIRT3 activity in a similar manner, resulting in abnormal mitochondrial protein acetylation in the heart and impaired cardiac function. Such heart disease candidates include inherited mitochondrial cardiomyopathies, diabetic and metabolic syndrome heart disease, acquired cardiac hypertrophy, age-related and ischemic heart disease, and heart failure (42, 71, 104, 105). For example, the ischemic heart results in a shift in redox state with accumulation of NADH (87), mirroring the consequential disturbance in energy equivalents in the FRDA heart.

Recent work has shown that exogenous treatment with NAD⁺ precursors can increase NAD⁺ levels in mitochondria, reduce protein acetylation, and activate sirtuins (58-61). We were surprised to observe that treating FXN KO mice with NR increased mitochondrial protein acetylation despite an increase in mitochondrial SIRT3 expression levels. NR-treatment may act to increase acetyl CoA levels by upregulated processing of acetate, pyruvate, and fatty acids via increased SIRT3 deacetylation of pyruvate dehydrogenase (PDH), acetyl coA synthase 2 (AceCS2), and the fatty acid oxidation enzymes (e.g. LCAD). This acetyl CoA would then be blocked at the TCA cycle due to reduced aconitase secondary to absence of FXN. Increased acetyl CoA would then favor acetylation via non-enzymatic acetylation of protein lysine residues (106).

Mitochondrial-targeted protein replacement therapy with TAT-FXN is effective at rescuing a murine model of FRDA with multiple tissue involvement (98). We were able to reduce mitochondrial protein acetylation in the FXN/SIRT3 DKO mice with TAT-FXN replacement therapy. This provides evidence that presence of SIRT3 deacetylase activity in the mitochondria

is not necessary to modulate acetylation levels. Most likely, acetylation went down in the presence of FXN because of a reduction in the burden of excess acetyl CoA that was able to enter the TCA cycle from increased aconitase activity (98). This finding that modulation of acetylation is not dependent on SIRT3 activity is of interest and applicable to other animal models of mitochondrial or metabolic heart disease and warrants further investigation.

Despite a modest reduction in mitochondrial protein acetylation, TAT-FXN therapy was not successful at alleviating heart failure, left ventricular remodeling or cardiac steatosis in the double knockout mice. This suggests that SIRT3 function is necessary to normalize cardiac function. For instance, ventricular tissue of FXN/SIRT3 DKO demonstrates myocardial lipid accumulation, which is not alleviated with TAT-FXN replacement therapy. This finding is not unsurprising considering others' findings that absence of SIRT3 leads to dysfunctional lipid metabolism. These results imply that inactive SIRT3 in the FXN KO heart may be the main contributor of dysfunctional lipid metabolism, due to its inability to deacetylate and activate targeted fatty acid oxidation enzymes, such as LCAD (42). However, because of our previous documentation that acetylation is negatively correlated with heart function, it would be of interest to determine if there is a dose-dependent response of acetylation and cellular and physiologic outcome to TAT-FXN replacement therapy. This could be achieved by pursuing trials of larger or more frequent doses of TAT-FXN in the double knockout mouse.

In conclusion, we demonstrate that loss of SIRT3 in the FXN KO heart leads to worse heart function and SIRT3 activity is necessary to rescue heart function in a murine model of FRDA cardiomyopathy. These results suggest that SIRT3 contributes to the pathophysiology of FRDA heart disease and may represent a therapeutic target to improve cardiac metabolism and physiologic function and prevent unremitting progressive heart disease.

Methods

Mouse breeding and genotyping. This study was approved by the Institutional Animal Care and Use Committee of Indiana University. We used site-specific Cre-lox recombination to carry out gene deletions of interest. We used FXN^{f/f} mice to create FXN KO mice that were homozygous for heart and skeletal muscle deletion of FXN (MCK-Cre: FXN KO), as previously published (55). We used SIRT3^{f/f} mice to create SIRT3 KO mice that were homozygous for heart and skeletal muscle deletion of SIRT3 (MCK-Cre: SIRT3 KO) as described by others (107). The double knockout, or FXN/SIRT3 DKO, mice were homozygous for both SIRT3 and FXN expression loss restricted to heart and skeletal muscle (MCK-Cre: FXN KO/SIRT3 KO). Data was collected at 10 weeks of age (± 5 days). Controls were age- and sex-matched healthy littermates (FXN^{f/f} or SIRT3^{f/f}, as indicated in text).

Lifespan, weight collection and mortality rate. Mice of each genotype were weighed twice weekly and natural death date recorded. Surgical stress-related mortality was determined by occurrence of spontaneous death in <10 minutes from right paratracheal skin incision under controlled anesthesia, and survival determined by survival of ≥ 10 minutes under equivalent conditions.

Echocardiography (ECHO). Mice were anesthetized with isoflurane and placed on a warming mat with continuous monitoring. Transthoracic ECHO images were obtained using a VisualSonics® 2100 ultrasound machine for small animal imaging and MS400 transducer (Fujifilm VisualSonics, Inc., Toronto, Canada). Functional parameters of the left ventricle and outflow tracts were measured using standard assessment techniques (108). Relative wall thickness (RWT) was calculated by $(2 * LVPWd) / LVIDd$ (109).

Cardiac Catheterization. Mice were anesthetized with isoflurane and placed on a warming mat with continuous monitoring. Pressure-volume loops were obtained directly using a 1.2 F microconductance catheter (Scisense, Transonic Systems Inc.), which was inserted into the right carotid artery through a small neck incision and advanced retrograde into the left ventricle. The ADVantage pressure volume system (Scisense, Transonic Systems Inc.) was used to acquire pressure, admittance, phase shift, and amplitude, and real time pressure-volume data was displayed and analyzed offline using specialized software (Labscribe 2, iWorx, Dover, NH).

Nicotinamide riboside therapy. FXN KO mice and healthy controls (n=6) were treated with oral gavage administration of nicotinamide riboside chloride (Niagen, ChromaDex, Inc.) at 500 mg/kg/day from 4 weeks of age until sacrifice at 10 weeks of age. Analysis with ECHO and catheterization as described above. Hearts were harvested the completion of study and subsequently processed or flash frozen for later analysis. Results were compared to untreated age- and sex-matched animals. NAD⁺ levels were measured using colorimetric detection of NAD⁺ concentration based on a standard curve and expressed as pmol/μg of protein (NAD⁺/NADH Assay Kit, Abcam ab65348).

TAT-FXN targeted protein replacement therapy. TAT-FXN was generated as previously published (98). FXN/SIRT3 DKO mice were dosed 2 days/week at 10mg/kg body weight via intraperitoneal route and compared to untreated age-matched FXN/SIRT3 DKO animals. FXN levels in heart tissue of treated animals were determined by ELISA within 4 hours of last drug dose (Human Frataxin ELISA Kit, Abcam ab176112).

Histology. Ventricular tissue selected for histology was fixed in 10% formalin and paraffin embedded. Histological analysis included hematoxylin and eosin (H&E) and Masson's trichrome to detect collagen as a measure of fibrosis. Collagen quantification was performed using ImageJ

(IJ1.46) (110) to measure percent area of tissue positively stained for collagen. Three to five 20x digital micrographs were obtained from each tissue section that underwent quantification studies.

Electron Microscopy (EM). Ventricular tissue selected for electron microscopy was fixed in 2.5% glutaraldehyde and underwent sectioning and uranyl acetate staining by the Electron Microscopy Center of Indiana University School of Medicine. Three separate sections from each animal strain were selected for quantification analysis. Quantification methods were similar to methods used in (111, 112) and our previous work (98). Abnormal mitochondria were identified as those containing electron-dense inclusions, cristae loss or dissolution, and/or collapsed or condensed cristae. Mitochondria and myofibril area was measured using ImageJ (IJ1.46).

Isolation of Cardiac Mitochondria. Mitochondrial isolation followed the method described in our previous work (9). Freshly harvested hearts were submerged in ice-cold mitochondrial isolation buffer (mannitol 220 mM, sucrose 70 mM, MOPS 5 mM, EGTA 2 mM, pH 7.0). Heart tissue was weighed, homogenized with Dounce tissue grinder, and then subjected to differential centrifugation. The cytosolic portion was reserved separately and the final mitochondrial pellet was resuspended in RIPA buffer and used immediately for western blotting or flash frozen for later analysis.

Antibodies and Western Blotting. Primary antibodies included anti-acetyl-lysine (Cell Signaling #9441), anti-SIRT3 (Cell Signaling #5490), anti-SOD2 (acetyl K68) (Abcam ab137037), anti-SOD2 (Cell Signaling #13141), anti-VDAC (Cell Signaling #4866), anti-GAPDH (Cell Signaling #5174), anti-FXN (generous gift of Grazia Isaya, Mayo Clinic, Rochester MN), and to the electron transport chain complexes: anti-CI-NDUFA9 (Abcam ab14713), anti-CII-SDHB (Abcam ab14714) and anti-CIII-UQCRCFS1 (Abcam ab14746). Band intensity was measured using ImageJ (IJ1.46) and analyzed with established methods (110, 113, 114).

Statistics. All calculations, analyses and graphs were performed using SigmaPlot (Systat Software, Inc.). Two groups were compared using a two-tailed student's t test for samples with equal variance. Three or more groups were compared using ANOVA and followed by the Holm-Sidak approach for multiple comparisons. Final data are presented as mean (\pm SD). Alpha was set at 0.05 and power at 0.800. A *p*-value of <0.05 was considered statistically significant.

CHAPTER 4

CONCLUSION

Heart disease exerts significant patient morbidity, mortality and cost burden to health care infrastructure in the United States (1). Heart failure, in particular, contributes much to this burden and little can be offered by way of treatment for this widely prevalent and etiologically diverse condition (2). Therefore, it is of utmost importance to illuminate common underlying mechanisms causing the cardiac dysfunction that leads to development of heart failure in order to develop effective therapies. Metabolic disturbance is one such common feature in cardiovascular disease, such as that which occurs in ischemia, diabetic cardiomyopathy, hypertrophy and heart failure, and has garnered relevant attention by researchers in recent years (115-118).

As cellular powerhouses, mitochondria serve as a site where the pathways of metabolism converge to generate vital energy needs for cell function. The heart, in particular, relies heavily on consistent energy generating capacity of the mitochondria. Mounting evidence suggests that mitochondrial dysfunction underlies the metabolic disruption that accompanies cardiovascular decline, underscoring the importance of mitochondrial failure as a pathogenic mechanism for heart disease progression (3, 4). For this reason, mitochondria have become a major focus in the investigation of cardiac disease in recent years and are poised to become a target of therapeutic intervention potentially for a vast spectrum of cardiac diseases.

Protein acetylation has gained recognition in recent years as an important post-translational processing mechanism to regulate cellular metabolism in response to shifting energy needs. The vast majority of mitochondria protein acetylation appears to be orchestrated by the NAD^+ -dependent deacetylase, SIRT3, which has the capacity to read and regulate the energy needs of the cell (119). It is not surprising that loss of SIRT3 activity leads to significant downstream consequences as the capacity of mitochondria to meet the cell's metabolic demands

fails in the absence of acetylation regulation (25, 39, 42, 59). Abnormally high levels of acetylation are observed in a range of cardiac diseases. For instance, human heart tissues from patients in heart failure demonstrate hyper-acetylation, as do mouse models of diabetic and mitochondrial cardiomyopathy (9, 104, 120, 121). This serves to illustrate that abnormal acetylation is occurring in diseased myocardium arising from distinct etiologies and is a shared pathologic feature amongst cardiovascular diseases.

A promising characteristic of SIRT3 is that its activity is modifiable via exogenous supplementation with NAD^+ precursors, nicotinamide riboside (NR) or nicotinamide mononucleotide (NMN). SIRT3, which requires NAD^+ as a cofactor, responds to a boost in mitochondrial NAD^+ content with increased deacetylase activity. This, in turn, leads to decreased acetylation levels, improved mitochondrial function and resultant cardioprotection (59, 60, 121). Taken together, mitochondrial protein lysine acetylation could serve as a modifiable target for therapies aimed to regulate cardiac metabolism in an attempt to alleviate the burden of heart disease.

The congenitally acquired condition of FRDA is a relentlessly progressive and fatal mitochondrial disease in which the majority of premature death occurs due to cardiac causes. Patients with FRDA develop hypertrophic cardiomyopathy leading to heart failure, culminating with death in the third or fourth decade of life. There is no effective cure. The FXN-deficient mitochondria have robust levels of acetylated proteins. This is likely due to inherently low levels of NAD^+ despite cellular energy deprivation, and high levels of acetyl CoA due to decreased activity of aconitase. Based on what we know of mitochondrial protein acetylation and the central role of SIRT3 in providing cardiac protection, I hypothesized that hyperacetylation of FXN deficient mitochondria leads to worsening of the mitochondrial function, and that this, then, translates to a decline in left ventricular dysfunction. The impact of hyper-acetylation on the outcome of FRDA heart disease had not been previously explored. The overarching purpose of my project was to investigate the relationship between acetylation and left ventricular function in

FRDA heart disease in order to determine whether deregulation of acetylation in the FRDA heart leads to worse cardiac outcome.

In Chapter 2, I used an established murine mouse model of FRDA heart disease (FXN KO) to follow the progression of heart dysfunction and the pattern of lysine acetylation as it proceeded through early- mid- and late-stage heart disease. I was able to document that FXN KO murine hearts mimic FRDA heart disease with onset of early diastolic dysfunction and hypertrophic cardiomyopathy progressing rapidly to decompensated, dilated systolic and diastolic heart failure. I also documented that mitochondrial protein acetylation in these hearts is progressive and tracks that of progressive cardiomyopathy. Most importantly, heart function and acetylation is connected by a strong negative correlation in the FXN KO heart. Findings in chapter 2 lead to the conclusion that abnormal acetylation contributes to the pathophysiology of heart disease in FRDA.

Further insights were gained into the link between metabolic disruption and the pathological process of cardiomyopathy due to FXN loss. First, there were findings of lipid metabolism dysfunction, evidenced by marked accumulation of lipids in the cardiomyocytes. This is likely related, at least in part, to increased acetylation of LCAD secondary to decreased activity of SIRT3. Interestingly, conditional loss of FXN leads to an inability to maintain normal thermogenesis in the face of a prolonged hypothermic insult. This finding is similar to that of murine models with loss MCAD or VLCAD, and thus suggests that cold intolerance is a product of the inability to properly metabolize lipids in the FXN KO heart. Second, measurable mitochondrial respiratory function is diminished in these hearts. This observation is not surprising based on the insult to Fe-S containing respiratory enzyme machinery resulting from loss of FXN, but may also be contributed to by loss of SIRT3 and its ability to modulate the activity of the electron transport chain via deacetylation of complex I. Further studies would be needed in order to determine the contribution of SIRT3 dysfunction in mitochondrial respiratory capacity. This could be accomplished by comparing mitochondrial respiratory rates in FXN KO and

FXN/SIRT3 DKO to determine whether a difference exists.

Because of the strong negative correlation between acetylation and cardiac function in FXN KO heart, I hypothesized that modifying acetylation levels would lead to changes in heart function. In Chapter 3, we generated a “double knockout” mouse with ablation of both FXN and SIRT3 in the heart (FXN/SIRT3 DKO) and I compared acetylation and heart function to the FXN KO mouse model. The mitochondrial acetylation of the FXN/SIRT3 DKO heart was markedly increased compared to age-matched FXN KO hearts. As expected, global measures of cardiac function and left ventricular remodeling in the FXN/SIRT3 DKO mouse were significantly worse compared to the FXN KO. Further, the FXN/SIRT3 DKO mice suffered significantly higher mortality rates in response to procedural stress and exhibited an accelerated rate of weight loss coincident with onset of cardiac decline, compared to FXN KO mice. Taken together, these findings lead to the conclusion that loss of SIRT3 in the FXN KO heart leads to worse heart function, in conjunction with increased mitochondrial protein acetylation.

I next asked whether reducing acetylation in the FXN KO heart would result in cardioprotection and attenuate previously observed cardiac pathology. I used exogenous therapy of the NAD⁺ precursor, nicotinamide riboside (NR) in order to stimulate SIRT3 deacetylase activity by providing enhanced cofactor bioavailability with the objective to reduce acetylation. I was surprised to discover that NR therapy lead to a modest increase in mitochondrial protein acetylation in the FXN KO hearts. This was despite its effectiveness at both 1) increasing NAD⁺ content and, 2) increasing mitochondrial SIRT3 expression. It is likely that increased SIRT3 deacetylation activity lead to increased acetyl CoA via its substrates pyruvate dehydrogenase (PDH), acetyl CoA synthase 2 (AceCS2), and the fatty acid oxidation enzymes (e.g. LCAD). The excess acetyl CoA would then be blocked from processing in the TCA cycle due to reduced aconitase secondary to absence of FXN. Acetyl CoA intermediates independently attach to lysine residues in the mitochondria. Such an increase in acetyl CoA, as suspected in this case, would push the balance in favor of acetylation. Further studies comparing measurements of acetyl CoA

in the NR-treated and untreated FXN KO hearts would be the next step in pursuing the mechanisms underlying these biochemical results. The modest increase in acetylation was accompanied by no change in heart function. These findings lead to the conclusion that SIRT3 activity alone is not sufficient to rescue heart function in the FXN KO in the face of increased levels of acetylation.

Because of the contrast in acetylation state between FXN KO and FXN/SIRT3 DKO mitochondria, I expected that replacing FXN expression in the FXN/SIRT3 DKO would lead to reduced acetylation. And, indeed, increasing FXN expression using a protein replacement therapy (TAT-FXN) in the FXN/SIRT3 DKO mouse lead to a modest reduction in mitochondrial protein acetylation. This provides evidence that while acetylation is regulated by SIRT3 in the FXN KO heart, it is not solely responsible for acetylation, and agrees with the findings above.

I then asked whether reducing acetylation in the FXN/SIRT3 DKO mice would improve cardiac pathology even in the absence of SIRT3. My objective was to begin to determine the contribution to left ventricular dysfunction in the FXN/SIRT3 DKO mouse attributable to SIRT3. Cardiac pathology in the TAT-FXN treated FXN/SIRT3 DKO mice was not improved compared to untreated animals. Taken together, these findings demonstrate that FXN expression is sufficient to modify acetylation and suggest that SIRT3 activity is necessary – but not sufficient – to improve heart function at a cellular and functional level in FXN-deficient hearts.

However, because TAT-FXN therapy in the study mice did not effectively result in reducing acetylation to SIRT3 KO levels, as would be expected in response to normalizing FXN expression levels, this leads me to speculate whether there is a dose-dependent response of acetylation to TAT-FXN therapy. Further studies trialing higher concentrations, more frequent and earlier dosing schedules would be of great interest to pursue. It would also be of interest to determine whether there is a certain level of mitochondrial protein acetylation that is able to elicit the most response in cardiac outcome. This could be achieved by titrating acetylation modification in FXN/SIRT3 DKO hearts and measuring impact on cardiac outcome.

Together, these findings provide novel insight into the molecular and physiologic basis underlying the mitochondrial cardiomyopathy of FRDA. These results suggest that both SIRT3 and acetylation play a contributory role leading to heart failure in FRDA. More studies are necessary in order to delineate the independent roles held by acetylation and SIRT3 and whether minimizing mitochondrial protein acetylation could mitigate left heart dysfunction in FRDA cardiomyopathy. Acetylation remains a promising therapeutic target in this childhood heart disease.

Appendix A

List of Definitions

+dP/dt = rate of pressure change in the ventricle

Respiratory control ratio (RCR) = indicates the tightness of the coupling between respiration and phosphorylation; the ratio of respiratory state 3 rate (ADP-stimulated respiration): state 4 rate (oxygen consumption in the absence of ADP or any metabolic poisons or inhibitors)

Tau (Mirsky) = time required for left ventricle pressure to fall to one-half of its value at end systolic pressure

Tau (Weiss) = regression of log*pressure

Appendix B

List of equations

$$-dP/dt = -\Delta\text{intra-ventricular pressure}/\Delta\text{time}$$

$$+dP/dt = +\Delta\text{intra-ventricular pressure}/\Delta\text{time}$$

$$\text{Rate of weight loss} = \text{median rate } (\Delta\text{mass (gm)}/\Delta\text{time (weeks)})$$

$$\text{RWT} = 2 * \text{LVPWd}/\text{LVIDd}$$

REFERENCES

1. Benjamin EJ, Blaha MJ, Chiuve SE, Cushman M, Das SR, Deo R, et al. Heart Disease and Stroke Statistics-2017 Update: A Report From the American Heart Association. *Circulation*. 2017;135(10):e146-e603.
2. Ziaeeian B, Fonarow GC. Epidemiology and aetiology of heart failure. *Nat Rev Cardiol*. 2016;13(6):368-78.
3. Brown DA, Perry JB, Allen ME, Sabbah HN, Stauffer BL, Shaikh SR, et al. Expert consensus document: Mitochondrial function as a therapeutic target in heart failure. *Nat Rev Cardiol*. 2017;14(4):238-50.
4. Neubauer S. The failing heart--an engine out of fuel. *N Engl J Med*. 2007;356(11):1140-51.
5. Pillai VB, Sundaresan NR, Jeevanandam V, Gupta MP. Mitochondrial SIRT3 and heart disease. *Cardiovasc Res*. 2010;88(2):250-6.
6. Rardin MJ, Newman JC, Held JM, Cusack MP, Sorensen DJ, Li B, et al. Label-free quantitative proteomics of the lysine acetylome in mitochondria identifies substrates of SIRT3 in metabolic pathways. *Proceedings of the National Academy of Sciences of the United States of America*. 2013;110(16):6601-6.
7. Koeppe A. Friedreich's ataxia: Pathology, pathogenesis, and molecular genetics. *Journal of the Neurological Sciences* (2011) 303 1–12.
8. Delatycki MB, Williamson R, Forrest SM. Friedreich ataxia: an overview. *J Med Genet*. 2000;37(1):1-8.
9. Gregory R, Wagner PMP, Clifford M, Babbey and R. Mark Payne. Friedreich's ataxia reveals a mechanism for coordinate regulation of oxidative metabolism via feedback inhibition of the SIRT3 deacetylase. *Human Molecular Genetics*. 2012;Vol. 21(No. 12):2688–97.
10. Schwer B, North BJ, Frye RA, Ott M, Verdin E. The human silent information regulator (Sir)2 homologue hSIRT3 is a mitochondrial nicotinamide adenine dinucleotide-dependent deacetylase. *The Journal of cell biology*. 2002;158(4):647-57.
11. Michishita E, Park JY, Burneskis JM, Barrett JC, Horikawa I. Evolutionarily conserved and nonconserved cellular localizations and functions of human SIRT proteins. *Molecular biology of the cell*. 2005;16(10):4623-35.
12. Anderson KA, Hirschey MD. Mitochondrial protein acetylation regulates metabolism. *Essays in biochemistry*. 2012;52:23-35.
13. Scott I, Webster BR, Li JH, Sack MN. Identification of a molecular component of the mitochondrial acetyltransferase programme: a novel role for GCN5L1. *Biochem J*. 2012;443(3):655-61.
14. Wagner GR, Payne RM. Widespread and enzyme-independent Nepsilon-acetylation and Nepsilon-succinylation of proteins in the chemical conditions of the mitochondrial matrix. *The Journal of biological chemistry*. 2013;288(40):29036-45.
15. Pougovkina O, te Brinke H, Ofman R, van Cruchten AG, Kulik W, Wanders RJ, et al. Mitochondrial protein acetylation is driven by acetyl-CoA from fatty acid oxidation. *Hum Mol Genet*. 2014;23(13):3513-22.
16. Bharathi SS, Zhang Y, Mohsen AW, Uppala R, Balasubramani M, Schreiber E, et al. Sirtuin 3 (SIRT3) protein regulates long-chain acyl-CoA dehydrogenase by deacetylating conserved lysines near the active site. *The Journal of biological chemistry*. 2013;288(47):33837-47.
17. Hirschey MD, Shimazu T, Goetzman E, Jing E, Schwer B, Lombard DB, et al. SIRT3 regulates mitochondrial fatty-acid oxidation by reversible enzyme deacetylation. *Nature*. 2010;464(7285):121-U37.

18. Ozden O, Park SH, Wagner BA, Yong Song H, Zhu Y, Vassilopoulos A, et al. SIRT3 deacetylates and increases pyruvate dehydrogenase activity in cancer cells. *Free radical biology & medicine*. 2014;76:163-72.
19. Schwer B, Bunkenborg J, Verdin RO, Andersen JS, Verdin E. Reversible lysine acetylation controls the activity of the mitochondrial enzyme acetyl-CoA synthetase 2. *Proceedings of the National Academy of Sciences of the United States of America*. 2006;103(27):10224-9.
20. Someya S, Yu W, Hallows WC, Xu J, Vann JM, Leeuwenburgh C, et al. Sirt3 mediates reduction of oxidative damage and prevention of age-related hearing loss under caloric restriction. *Cell*. 2010;143(5):802-12.
21. Cimen H, Han MJ, Yang Y, Tong Q, Koc H, Koc EC. Regulation of succinate dehydrogenase activity by SIRT3 in mammalian mitochondria. *Biochemistry*. 2010;49(2):304-11.
22. Finley LW, Haas W, Desquiret-Dumas V, Wallace DC, Procaccio V, Gygi SP, et al. Succinate dehydrogenase is a direct target of sirtuin 3 deacetylase activity. *PLoS One*. 2011;6(8):e23295.
23. Ahn BH, Kim HS, Song SW, Lee IH, Liu J, Vassilopoulos A, et al. A role for the mitochondrial deacetylase Sirt3 in regulating energy homeostasis. *Proceedings of the National Academy of Sciences of the United States of America*. 2008;105(38):14447-52.
24. Shinmura K, Tamaki K, Sano M, Nakashima-Kamimura N, Wolf AM, Amo T, et al. Caloric restriction primes mitochondria for ischemic stress by deacetylating specific mitochondrial proteins of the electron transport chain. *Circulation research*. 2011;109(4):396-406.
25. Hafner AV, Dai J, Gomes AP, Xiao CY, Palmeira CM, Rosenzweig A, et al. Regulation of the mPTP by SIRT3-mediated deacetylation of CypD at lysine 166 suppresses age-related cardiac hypertrophy. *Aging*. 2010;2(12):914-23.
26. Fernandes J, Weddle A, Kinter CS, Humphries KM, Mather T, Szweda LI, et al. Lysine Acetylation Activates Mitochondrial Aconitase in the Heart. *Biochemistry*. 2015;54(25):4008-18.
27. Vassilopoulos A, et al. "SIRT3 Deacetylates ATP Synthase F1 Complex Proteins in Response to Nutrient-and Exercise-Induced Stress." *Antioxidants & redox signaling* (2013).
28. Bao J, Scott I, Lu Z, Pang L, Dimond CC, Gius D, et al. SIRT3 is regulated by nutrient excess and modulates hepatic susceptibility to lipotoxicity. *Free radical biology & medicine*. 2010;49(7):1230-7.
29. Bong-Hyun Ahn H-SK, Shiwei Song, In Hye Lee, Jie Liu, Athanassios Vassilopoulos, Chu-Xia Deng, and Finkel, a. T. (2008) A role for the mitochondrial deacetylase Sirt3 in regulating energy homeostasis, *PNAS* 105, 14447-14452. A role for the mitochondrial deacetylase Sirt3 in regulating energy homeostasis, *PNAS* (2008) 105, :14447-52.
30. Hallows WC, Lee S, Denu JM. Sirtuins deacetylate and activate mammalian acetyl-CoA synthetases. *Proceedings of the National Academy of Sciences of the United States of America*. 2006;103(27):10230-5.
31. Shimazu T, Hirschey MD, Hua L, Dittenhafer-Reed KE, Schwer B, Lombard DB, et al. SIRT3 deacetylates mitochondrial 3-hydroxy-3-methylglutaryl CoA synthase 2 and regulates ketone body production. *Cell Metab*. 2010;12(6):654-61.
32. Shulga N, Wilson-Smith R, Pastorino JG. Sirtuin-3 deacetylation of cyclophilin D induces dissociation of hexokinase II from the mitochondria. *J Cell Sci*. 2010;123(Pt 6):894-902.
33. Jing EX, O'Neill BT, Rardin MJ, Kleinridders A, Ilkeyeva OR, Ussar S, et al. Sirt3 Regulates Metabolic Flexibility of Skeletal Muscle Through Reversible Enzymatic Deacetylation. *Diabetes*. 2013;62(10):3404-17.
34. Chen Y, Zhang J, Lin Y, Lei Q, Guan KL, Zhao S, et al. Tumour suppressor SIRT3 deacetylates and activates manganese superoxide dismutase to scavenge ROS. *EMBO reports*. 2011;12(6):534-41.
35. Qiu X, Brown K, Hirschey MD, Verdin E, Chen D. Calorie restriction reduces oxidative stress by SIRT3-mediated SOD2 activation. *Cell Metab*. 2010;12(6):662-7.

36. Tao R, Coleman MC, Pennington JD, Ozden O, Park SH, Jiang H, et al. Sirt3-mediated deacetylation of evolutionarily conserved lysine 122 regulates MnSOD activity in response to stress. *Molecular cell*. 2010;40(6):893-904.
37. Cheng Y, Ren X, Gowda AS, Shan Y, Zhang L, Yuan YS, et al. Interaction of Sirt3 with OGG1 contributes to repair of mitochondrial DNA and protects from apoptotic cell death under oxidative stress. *Cell Death Dis*. 2013;4:e731.
38. Winnik S, Auwerx J, Sinclair DA, Matter CM. Protective effects of sirtuins in cardiovascular diseases: from bench to bedside. *Eur Heart J*. 2015;36(48):3404-12.
39. Chen CJ, Fu YC, Yu W, Wang W. SIRT3 protects cardiomyocytes from oxidative stress-mediated cell death by activating NF-kappaB. *Biochemical and biophysical research communications*. 2013;430(2):798-803.
40. Cheung KG, Cole LK, Xiang B, Chen K, Ma X, Myal Y, et al. Sirtuin-3 (SIRT3) Protein Attenuates Doxorubicin-induced Oxidative Stress and Improves Mitochondrial Respiration in H9c2 Cardiomyocytes. *The Journal of biological chemistry*. 2015;290(17):10981-93.
41. Tseng AH, Shieh SS, Wang DL. SIRT3 deacetylates FOXO3 to protect mitochondria against oxidative damage. *Free radical biology & medicine*. 2013;63:222-34.
42. Chen T, Liu J, Li N, Wang S, Liu H, Li J, et al. Mouse SIRT3 attenuates hypertrophy-related lipid accumulation in the heart through the deacetylation of LCAD. *PLoS One*. 2015;10(3):e0118909.
43. Sundaresan NR, Gupta M, Kim G, Rajamohan SB, Isbatan A, Gupta MP. Sirt3 blocks the cardiac hypertrophic response by augmenting Foxo3a-dependent antioxidant defense mechanisms in mice. *Journal of Clinical Investigation*. 2009;119(9):2758-71.
44. Koentges C, Pfeil K, Schnick T, Wiese S, Dahlbock R, Cimolai MC, et al. SIRT3 deficiency impairs mitochondrial and contractile function in the heart. *Basic research in cardiology*. 2015;110(4):36.
45. Porter GA, Urciuoli WR, Brookes PS, Nadtochiy SM. SIRT3 deficiency exacerbates ischemia-reperfusion injury: implication for aged hearts. *American journal of physiology Heart and circulatory physiology*. 2014;306(12):H1602-9.
46. Campuzano V, Montermini L, Molto MD, Pianese L, Cousse M, Cavalcanti F, et al. Friedreich's ataxia: autosomal recessive disease caused by an intronic GAA triplet repeat expansion. *Science*. 1996;271(5254):1423-7.
47. Harding AE. Friedreich's ataxia: a clinical and genetic study of 90 families with an analysis of early diagnostic criteria and intrafamilial clustering of clinical features. *Brain* 1981;104.
48. Tsou AY, Paulsen EK, Lagedrost SJ, Perlman SL, Mathews KD, Wilmot GR, et al. Mortality in Friedreich ataxia. *J Neurol Sci*. 2011;307(1-2):46-9.
49. Frank Weidemann CR, Bart Bijnens, Stefan Störk, Ruta Jasaityte, Jan Dhooge, Aigul Baltabaeva, George Sutherland, Jörg B. Schulz and Thomas Meier. *The Heart in Friedreich Ataxia: Definition of Cardiomyopathy, Disease Severity, and Correlation With Neurological Symptoms*. *Circulation*. 2012;125:1626-34.
50. Pandolfo. FRaM. Cardiomyopathy in Friedreich's Ataxia. *Acta Neurol Belg*. 2011, ;111, :183-7.
51. Pandolfo M, Pastore A. The pathogenesis of Friedreich ataxia and the structure and function of frataxin. *Journal of Neurology*. 2009;256([Suppl 1]):9-17.
52. Bulteau AL, O'Neill HA, Kennedy MC, Ikeda-Saito M, Isaya G, Szweda LI. Frataxin acts as an iron chaperone protein to modulate mitochondrial aconitase activity. *Science*. 2004;305(5681):242-5.
53. Bunse M, Bit-Avragim N, Riefflin A, Perrot A, Schmidt O, Kreuz FR, et al. Cardiac energetics correlates to myocardial hypertrophy in Friedreich's ataxia. *Ann Neurol*. 2003;53(1):121-3.

54. Koutnikova H, Campuzano V, Foury F, Dolle P, Cazzalini O, Koenig M. Studies of human, mouse and yeast homologues indicate a mitochondrial function for frataxin. *Nat Genet.* 1997;16(4):345-51.
55. Hélène Puccio DS, Mireille Cossée, Paola Criqui-Filipe, Francesco Tiziano, Judith Melki, Colette Hindelang, Robert Matyas, Pierre Rustin & Michel Koenig. . Mouse models for Friedreich ataxia exhibit cardiomyopathy, sensory nerve defect and Fe-S enzyme deficiency followed by intramitochondrial iron deposits. . *Nature Genetics* 2001;volume 27(February).
56. Hart PE, Lodi R, Rajagopalan B, Bradley JL, Crilley JG, Turner C, et al. Antioxidant treatment of patients with Friedreich ataxia - Four-year follow-up. *Archives of Neurology.* 2005;62(4):621-6.
57. Mori V, Amici A, Mazzola F, Di Stefano M, Conforti L, Magni G, et al. Metabolic profiling of alternative NAD biosynthetic routes in mouse tissues. *PLoS One.* 2014;9(11):e113939.
58. Canto C, Houtkooper RH, Pirinen E, Youn DY, Oosterveer MH, Cen Y, et al. The NAD(+) precursor nicotinamide riboside enhances oxidative metabolism and protects against high-fat diet-induced obesity. *Cell Metab.* 2012;15(6):838-47.
59. Pillai VB, Sundaresan NR, Kim G, Gupta M, Rajamohan SB, Pillai JB, et al. Exogenous NAD blocks cardiac hypertrophic response via activation of the SIRT3-LKB1-AMP-activated kinase pathway. *The Journal of biological chemistry.* 2010;285(5):3133-44.
60. Yamamoto T, Byun J, Zhai P, Ikeda Y, Oka S, Sadoshima J. Nicotinamide mononucleotide, an intermediate of NAD⁺ synthesis, protects the heart from ischemia and reperfusion. *PLoS One.* 2014;9(6):e98972.
61. Yoshino J, et al. "Nicotinamide Mononucleotide, a Key NAD⁺ Intermediate, Treats the Pathophysiology of Diet-and Age-Induced Diabetes in Mice." *Cell metabolism* (2011): ;14.(4):528-36.
62. Stram AR WG, Pride PM, Fogler BD, Hirschey MD, Payne RM. Progressive Mitochondrial Protein Lysine Acetylation and Heart Failure in a Model of Friedreich's Ataxia Cardiomyopathy. *PLoS one.* 2017;12(5):e0178354.
63. Mazumder PK, O'Neill BT, Roberts MW, Buchanan J, Yun UJ, Cooksey RC, et al. Impaired cardiac efficiency and increased fatty acid oxidation in insulin-resistant ob/ob mouse hearts. *Diabetes.* 2004;53(9):2366-74.
64. Christoffersen C, Bollano E, Lindegaard ML, Bartels ED, Goetze JP, Andersen CB, et al. Cardiac lipid accumulation associated with diastolic dysfunction in obese mice. *Endocrinology.* 2003;144(8):3483-90.
65. Turer AT, Stevens RD, Bain JR, Muehlbauer MJ, van der Westhuizen J, Mathew JP, et al. Metabolomic profiling reveals distinct patterns of myocardial substrate use in humans with coronary artery disease or left ventricular dysfunction during surgical ischemia/reperfusion. *Circulation.* 2009;119(13):1736-46.
66. Doenst T, Nguyen TD, Abel ED. Cardiac metabolism in heart failure: implications beyond ATP production. *Circulation research.* 2013;113(6):709-24.
67. Hsu YH, Yogasundaram H, Parajuli N, Valtuille L, Sergi C, Oudit GY. MELAS syndrome and cardiomyopathy: linking mitochondrial function to heart failure pathogenesis. *Heart Fail Rev.* 2016;21(1):103-16.
68. Huss JM, Kelly DP. Mitochondrial energy metabolism in heart failure: a question of balance. *J Clin Invest.* 2005;115(3):547-55.
69. Zhang Y BS, Rardin MJ, Uppala R, Verdin E, Gibson BW, Goetzman E. SIRT3 and SIRT5 Regulate the Enzyme Activity and Cardiolipin Binding of Very Long- Chain Acyl-CoA Dehydrogenase. *PLoS One.* 2015;Mar 26;10(3):e0122297.
70. Ahn BH, Kim HS, Song S, Lee IH, Liu J, Vassilopoulos A, et al. A role for the mitochondrial deacetylase Sirt3 in regulating energy homeostasis. *Proceedings of the National Academy of Sciences of the United States of America.* 2008;105(38):14447-52.

71. Alrob OA, Sankaralingam S, Ma C, Wagg CS, Fillmore N, Jaswal JS, et al. Obesity-induced lysine acetylation increases cardiac fatty acid oxidation and impairs insulin signalling. *Cardiovasc Res.* 2014;103(4):485-97.
72. Sundaresan NR, Gupta M, Kim G, Rajamohan SB, Isbatan A, Gupta MP. Sirt3 blocks the cardiac hypertrophic response by augmenting Foxo3a-dependent antioxidant defense mechanisms in mice. *J Clin Invest.* 2009;119(9):2758-71.
73. Tsai CL, Barondeau DP. Human frataxin is an allosteric switch that activates the Fe-S cluster biosynthetic complex. *Biochemistry.* 2010;49(43):9132-9.
74. Lodi R, Rajagopalan B, Blamire AM, Cooper JM, Davies CH, Bradley JL, et al. Cardiac energetics are abnormal in Friedreich ataxia patients in the absence of cardiac dysfunction and hypertrophy: An in vivo (31)P magnetic resonance spectroscopy study. *Cardiovascular Research.* 2001;52(1):111-9.
75. Schulz JB, Dehmer T, Schols L, Mende H, Hardt C, Vorgerd M, et al. Oxidative stress in patients with Friedreich ataxia. *Neurology.* 2000;55(11):1719-21.
76. Wagner GR, Pride PM, Babbey CM, Payne RM. Friedreich's ataxia reveals a mechanism for coordinate regulation of oxidative metabolism via feedback inhibition of the SIRT3 deacetylase. *Hum Mol Genet.* 2012;21(12):2688-97.
77. Seznec H SD, Monassier L, Criqui-Filipe P, Gansmuller A, Rustin P, Koenig M, Puccio H. . Idebenone delays the onset of cardiac functional alteration without correction of Fe-S enzymes deficit in a mouse model for Friedreich ataxia. . *Hum Mol Genet* 2004 May 15;13(10)::1017-24. .
78. Wagner GR, IUPUI ScholarWorks. Identification and characterization of altered mitochondrial protein acetylation in Friedreich's ataxia cardiomyopathy [2 665 mb]2013. Available from: <http://hdl.handle.net/1805/4209>.
79. Puccio H, Simon D, Cossee M, Criqui-Filipe P, Tiziano F, Melki J, et al. Mouse models for Friedreich ataxia exhibit cardiomyopathy, sensory nerve defect and Fe-S enzyme deficiency followed by intramitochondrial iron deposits. *NatGenet.* 2001;27(2):181-6.
80. Schmucker S, Martelli A, Colin F, Page A, Wattenhofer-Donze M, Reutenauer L, et al. Mammalian frataxin: an essential function for cellular viability through an interaction with a preformed ISCU/NFS1/ISD11 iron-sulfur assembly complex. *PLoS One.* 2011;6(1):e16199.
81. Choudhary C, Kumar C, Gnad F, Nielsen ML, Rehman M, Walther TC, et al. Lysine acetylation targets protein complexes and co-regulates major cellular functions. *Science.* 2009;325(5942):834-40.
82. Hirschey MD, Shimazu T, Goetzman E, Jing E, Schwer B, Lombard DB, et al. SIRT3 regulates mitochondrial fatty-acid oxidation by reversible enzyme deacetylation. *Nature.* 2010;464(7285):121-5.
83. Vyas PM, Tomamichel WJ, Pride PM, Babbey CM, Wang Q, Mercier J, et al. A TAT-Frataxin fusion protein increases lifespan and cardiac function in a conditional Friedreich's ataxia mouse model. *Human Molecular Genetics.* 2012;21(6):1230-47.
84. Tolwani RJ, Hamm DA, Tian L, Sharer JD, Vockley J, Rinaldo P, et al. Medium-chain acyl-CoA dehydrogenase deficiency in gene-targeted mice. *PLoS Genet.* 2005;1(2):e23.
85. Xiong D, He H, James J, Tokunaga C, Powers C, Huang Y, et al. Cardiac-specific VLCAD deficiency induces dilated cardiomyopathy and cold intolerance. *American journal of physiology Heart and circulatory physiology.* 2014;306(3):H326-38.
86. Rotig A, de Lonlay P, Chretien D, Foury F, Koenig M, Sidi D, et al. Aconitase and mitochondrial iron-sulphur protein deficiency in Friedreich ataxia. *Nat Genet.* 1997;17(2):215-7.
87. Di Lisa F, Menabo R, Canton M, Barile M, Bernardi P. Opening of the mitochondrial permeability transition pore causes depletion of mitochondrial and cytosolic NAD⁺ and is a causative event in the death of myocytes in postischemic reperfusion of the heart. *The Journal of biological chemistry.* 2001;276(4):2571-5.

88. Koitabashi N, Bedja D, Zaiman AL, Pinto YM, Zhang M, Gabrielson KL, et al. Avoidance of transient cardiomyopathy in cardiomyocyte-targeted tamoxifen-induced MerCreMer gene deletion models. *Circ Res.* 2009;105(1):12-5.
89. Zhao S, Xu W, Jiang W, Yu W, Lin Y, Zhang T, et al. Regulation of cellular metabolism by protein lysine acetylation. *Science.* 2010;327(5968):1000-4.
90. Menzies KJ, Zhang H, Katsyuba E, Auwerx J. Protein acetylation in metabolism - metabolites and cofactors. *Nat Rev Endocrinol.* 2016;12(1):43-60.
91. Fukushima A, Lopaschuk GD. Acetylation control of cardiac fatty acid beta-oxidation and energy metabolism in obesity, diabetes, and heart failure. *Biochimica et biophysica acta.* 2016;1862(12):2211-20.
92. Abo Alrob O, Lopaschuk GD. Role of CoA and acetyl-CoA in regulating cardiac fatty acid and glucose oxidation. *Biochem Soc Trans.* 2014;42(4):1043-51.
93. Sol EM, Wagner SA, Weinert BT, Kumar A, Kim HS, Deng CX, et al. Proteomic investigations of lysine acetylation identify diverse substrates of mitochondrial deacetylase sirt3. *PLoS One.* 2012;7(12):e50545.
94. Hallows WC, Albaugh BN, Denu JM. Where in the cell is SIRT3?--functional localization of an NAD⁺-dependent protein deacetylase. *Biochem J.* 2008;411(2):e11-3.
95. Sundaresan NR, Samant SA, Pillai VB, Rajamohan SB, Gupta MP. SIRT3 is a stress-responsive deacetylase in cardiomyocytes that protects cells from stress-mediated cell death by deacetylation of Ku70. *Mol Cell Biol.* 2008;28(20):6384-401.
96. Iwahara T, Bonasio R, Narendra V, Reinberg D. SIRT3 functions in the nucleus in the control of stress-related gene expression. *Mol Cell Biol.* 2012;32(24):5022-34.
97. Cooper HM, Spelbrink JN. The human SIRT3 protein deacetylase is exclusively mitochondrial. *Biochem J.* 2008;411(2):279-85.
98. Vyas PM, Tomamichel WJ, Pride PM, Babbey CM, Wang QJ, Mercier J, et al. A TAT-Frataxin fusion protein increases lifespan and cardiac function in a conditional Friedreich's ataxia mouse model. *Human Molecular Genetics.* 2012;21(6):1230-47.
99. Krenning G, Zeisberg EM, Kalluri R. The origin of fibroblasts and mechanism of cardiac fibrosis. *J Cell Physiol.* 2010;225(3):631-7.
100. Zhou YT, Grayburn P, Karim A, Shimabukuro M, Higa M, Baetens D, et al. Lipotoxic heart disease in obese rats: implications for human obesity. *Proceedings of the National Academy of Sciences of the United States of America.* 2000;97(4):1784-9.
101. Chiu HC, Kovacs A, Ford DA, Hsu FF, Garcia R, Herrero P, et al. A novel mouse model of lipotoxic cardiomyopathy. *J Clin Invest.* 2001;107(7):813-22.
102. D'Souza K, Nzirorera C, Kienesberger PC. Lipid metabolism and signaling in cardiac lipotoxicity. *Biochimica et biophysica acta.* 2016;1861(10):1513-24.
103. Goldberg IJ, Trent CM, Schulze PC. Lipid metabolism and toxicity in the heart. *Cell Metab.* 2012;15(6):805-12.
104. Karamanlidis G, Lee CF, Garcia-Menendez L, Kolwicz SC, Jr., Suthammarak W, Gong G, et al. Mitochondrial complex I deficiency increases protein acetylation and accelerates heart failure. *Cell Metab.* 2013;18(2):239-50.
105. Grillon JM, Johnson KR, Kotlo K, Danziger RS. Non-histone lysine acetylated proteins in heart failure. *Biochimica et biophysica acta.* 2012;1822(4):607-14.
106. Guarente L. The logic linking protein acetylation and metabolism. *Cell Metab.* 2011;14(2):151-3.
107. Lombard DB, Alt FW, Cheng HL, Bunkenborg J, Streeper RS, Mostoslavsky R, et al. Mammalian Sir2 homolog SIRT3 regulates global mitochondrial lysine acetylation. *Mol Cell Biol.* 2007;27(24):8807-14.
108. Jörg Stypmann MAE, Clemens Troatz, Markus Rothenburger, Lars Eckardt and Klaus Tiemann. . Echocardiographic assessment of global left ventricular function in mice. . *Lab Anim* 2009 43:(127).

109. Lang RM, Bierig M, Devereux RB, Flachskampf FA, Foster E, Pellikka PA, et al. Recommendations for chamber quantification: a report from the American Society of Echocardiography's Guidelines and Standards Committee and the Chamber Quantification Writing Group, developed in conjunction with the European Association of Echocardiography, a branch of the European Society of Cardiology. *J Am Soc Echocardiogr.* 2005;18(12):1440-63.
110. Rasband WS. *Image J*, . Bethesda, Maryland, USA,: U.S. National Institutes of Health; 1997-2015. p. <http://imagej.nih.gov/ij/>.
111. Birk AV, Liu S, Soong Y, Mills W, Singh P, Warren JD, et al. The mitochondrial-targeted compound SS-31 re-energizes ischemic mitochondria by interacting with cardiolipin. *J Am Soc Nephrol.* 2013;24(8):1250-61.
112. Lewis W, Grupp IL, Grupp G, Hoit B, Morris R, Samarel AM, et al. Cardiac dysfunction occurs in the HIV-1 transgenic mouse treated with zidovudine. *Lab Invest.* 2000;80(2):187-97.
113. WS FTaR. *ImageJ User Guide — IJ 1.46 2010-2012* [Available from: imagej.nih.gov/ij/docs/guide/].
114. Miller L. *Analyzing Gels and Western Blots using Image J 2010* [Available from: <http://lukemiller.org/index.php/2010/11/analyzing-gels-and-western-blots-with-image-j/>].
115. Ingwall JS. Energy metabolism in heart failure and remodelling. *Cardiovasc Res.* 2009;81(3):412-9.
116. Stanley WC. Myocardial energy metabolism during ischemia and the mechanisms of metabolic therapies. *J Cardiovasc Pharmacol Ther.* 2004;9 Suppl 1:S31-45.
117. An D, Rodrigues B. Role of changes in cardiac metabolism in development of diabetic cardiomyopathy. *American journal of physiology Heart and circulatory physiology.* 2006;291(4):H1489-506.
118. Lai L, Leone TC, Keller MP, Martin OJ, Broman AT, Nigro J, et al. Energy metabolic reprogramming in the hypertrophied and early stage failing heart: a multisystems approach. *Circ Heart Fail.* 2014;7(6):1022-31.
119. Sack MN. The role of SIRT3 in mitochondrial homeostasis and cardiac adaptation to hypertrophy and aging. *Journal of molecular and cellular cardiology.* 2012;52(3):520-5.
120. Vadvalkar SS, Baily CN, Matsuzaki S, West M, Tesiram YA, Humphries KM. Metabolic inflexibility and protein lysine acetylation in heart mitochondria of a chronic model of type 1 diabetes. *Biochem J.* 2013;449(1):253-61.
121. Lee CF, Chavez JD, Garcia-Menendez L, Choi Y, Roe ND, Chiao YA, et al. Normalization of NAD⁺ Redox Balance as a Therapy for Heart Failure. *Circulation.* 2016;134(12):883-94.

CURRICULUM VITAE

Amanda R. Stram

POSITION TITLE

Resident Physician, Department of
Surgery
Indiana University School of Medicine

EDUCATION AND TRAINING

Institution and Location	DEGREE	MM/YY	FIELD OF STUDY
University of Wisconsin-Madison, Madison, WI	B.S.	05/04	Natural Sciences, Genetics
Boston University School of Medicine, Boston, MA	M.A.	09/07	Medical Sciences
Indiana University School of Medicine, Indianapolis, IN	M.D.	05/11	Medicine
Indiana University, Indianapolis, IN	Ph.D.	09/17	Cellular and Integrative Physiology

A. Positions

ACTIVITY/ OCCUPATION	BEGIN DATE (mm/yy)	END DATE (mm/yy)	FIELD	INSTITUTION/ COMPANY	SUPERVISOR/ EMPLOYER
Research Technician	2004	2005	Department of Medical Oncology	Dana-Farber Cancer Institute	William Kaelin, MD and James Brugarolas, MD
Volunteer Project Coordinator and Medical Assistant	2006	2007	Health Care	Boston Healthcare for the Homeless Program	Community HealthCorps
Intern and Surgical Resident	2011	date	Surgery	Department of General Surgery	Indiana University School of Medicine

B. Honors and Awards

- New Investigator Travel Award, BCVS Scientific Sessions 2014
- Carl H. McCaskey Award, American College of Surgeons, Indiana Chapter, 2014
- Best of AHA Specialty Conferences, AHA Scientific Sessions 2014
- Scanlan/Women in Thoracic Surgery Traveling Mentorship Award, 2015
- NIH Loan Repayment Program Award Recipient (2014-2016)

C. Academic and Professional Activity

Teaching

May-Aug 2014	Supervising and mentoring the research project of a senior medical student during a 12-week IUSM Student Research Program in Academic Medicine
August-October 2016	Epic medical record system physician instructor and trainer. Responsible for teaching a medical record system in lecture-based classes of physicians and providing hands-on training prior to hospital-wide implementation.

Grant Support

08/04/2015-08/03/2017
 NIH/NHLBI #F31HL126489
 The role of mitochondrial protein acetylation in left ventricular function.
 Role: Principle Investigator

Selected Publications

Peer Reviewed Publications

Stram AR, Payne RM. Post-translational modifications in mitochondria: protein signaling in the powerhouse. *Cell Mol Life Sci*. 2016 Nov;73(21):4063-73. doi: 10.1007/s00018-016-2280-4. Review. PubMed PMID: 27233499; PubMed Central PMCID: PMC5045789.

Stram, Amanda R., et al. "Progressive mitochondrial protein lysine acetylation and heart failure in a model of Friedreich's ataxia cardiomyopathy." *PloS one* 12.5 (2017): e0178354.

Oral Presentations

AR Stram. Mitochondrial protein hyperacetylation is associated with early diastolic dysfunction in a model of Friedreich's ataxia hypertrophic cardiomyopathy. *International Ataxia Research Conference*, March 2015

Stram, Amanda R., P. Melanie Pride, and R. Mark Payne. "NAD+ replacement therapy with nicotinamide riboside does not improve cardiac function in a model of mitochondrial heart disease." *The FASEB Journal* 31.1 Supplement (2017): 602-15.

Abstracts

Stram AR, Wagner GR, Pride PM, Payne RM. Progressive Mitochondrial Protein Acetylation and Microsteatosis is Associated with Diastolic Dysfunction in a Hypertrophic Cardiomyopathy Model. *Basic Cardiovascular Sciences Scientific Sessions*, July 2014 (abstract)

Stram AR, Wagner GR, Fogler BD, Pride PM, Payne RM. Mitochondrial Protein Hyperacetylation is associated with Early Diastolic Dysfunction in a Model of Friedreich's Ataxia Cardiomyopathy. *7th Annual Friedreich's Ataxia Symposium*, October 2014 (abstract)

A Stram; G Wagner; S Messina-Graham; P Pride; H Broxmeyer; R Payne. Mitochondrial Protein Hyperacetylation is associated with Early Diastolic Dysfunction in a Model of Hypertrophic Cardiomyopathy. *2015 Keystone Symposia Conference: Mitochondria, Metabolism and Heart Failure*. (abstract)